GeroScience
https://doi.org/10.1007/s11357-021-00355-9

ORIGINAL ARTICLE

Acute cognitive impairment after traumatic brain injury predicts the occurrence of brain atrophy patterns similar to those observed in Alzheimer's disease

Kenneth A. Rostowsky · Andrei Irimia · for the Alzheimer's Disease Neuroimaging Initiative

Received: 15 October 2020 / Accepted: 10 March 2021

Abstract Traumatic brain injuries (TBIs) are often followed by persistent structural brain alterations and by cognitive sequalae, including memory deficits, reduced neural processing speed, impaired social function, and decision-making difficulties. Although mild TBI (mTBI) is a risk factor for Alzheimer's disease (AD), the extent to which these conditions share patterns of macroscale neurodegeneration has not been quantified. Comparing such patterns can not only reveal how the neurodegenerative trajectories of TBI and AD are similar, but may also identify brain atrophy features which can be leveraged to prognosticate AD risk after TBI. The primary aim of this study is to systematically map how TBI affects white matter (WM) and gray matter (GM) properties in AD-analogous patterns. Our findings identify substantial similarities in the regional macroscale neurodegeneration patterns associated with mTBI and AD. In cerebral GM, such similarities are most extensive in brain areas involved in memory and executive function, such as the temporal poles and orbitofrontal cortices, respectively. Our results indicate that the spatial pattern of cerebral WM degradation observed in AD is broadly similar to the pattern of diffuse axonal injury observed in TBI, which frequently affects WM structures like the fornix, corpus callosum, and corona radiata. Using machine learning, we find that the severity of AD-like brain changes observed during the chronic stage of mTBI can be accurately prognosticated based on acute assessments of post-traumatic mild cognitive impairment. These findings suggest that acute post-traumatic cognitive impairment predicts the magnitude of AD-like brain atrophy, which is itself associated with AD risk.

Keywords Traumatic brain injury · Alzheimer's disease · Mild cognitive impairment · Neuroimaging

Abbreviations

ACR	Anterior corona radiata
AD	Alzheimer's disease
ADNI	Alzheimer's Disease Neuroimaging Initiative
AIC	Anterior internal capsule
ApoE	Apolipoprotein E
Aβ	Amyloid beta
BCC	Body of the corpus callosum
BCF	Body and column of the fornix
CAA	Cerebral amyloid angiopathy
CB	Cingulum bundle
CC	Corpus callosum
CDR	Clinical dementia rating
CDR-SB	Clinical dementia rating sum of boxes
CF	Crus of the fornix

K. A. Rostowsky · A. Irimia
Ethel Percy Andrus Gerontology Center, Leonard Davis School of Gerontology, University of Southern California, Los Angeles, CA, USA

A. Irimia (✉)
Corwin D. Denney Research Center, Department of Biomedical Engineering, Viterbi School of Engineering, University of Southern California, Los Angeles, CA, USA
e-mail: irimia@usc.edu

Published online: 26 April 2021

CI	Confidence interval
CMB	Cerebral microbleed
CP	Cerebral peduncle
CST	Corticospinal tract
CT	Computed tomography
DAI	Diffuse axonal injury
DL	Deep learning
DMN	Default mode network
dMRI	Diffusion magnetic resonance imaging
DTI	Diffusion tensor imaging
DWI	Diffusion weighted imaging
EC	External capsule
FA	Fractional anisotropy
FLAIR	Fluid-attenuated inversion recovery
FN	False negative
FP	False positive
FSL	FMRIB software library
FWER	Family-wise error rate
GCC	Genu of the corpus callosum
GCS	Glasgow Coma Scale
GLM	General linear model
GM	Gray matter
GRE	Gradient-recalled echo
HC	Healthy control
ICbP	Inferior cerebellar peduncle
ICBM	International Consortium of Brain Mapping
IFG	Inferior frontal gyrus
IFOF	Inferior fronto-occipital fasciculus
ISDA	Iterative single data algorithm
JHU	Johns Hopkins University
LOC	Loss of consciousness
MCC	Matthews' correlation coefficient
MCI	Mild cognitive impairment
ML	Medial lemniscus
MMSE	Mini mental state examination
MNI	Montreal Neurological Institute
MoCA	Montreal cognitive assessment
MP-RAGE	Magnetization-prepared rapid acquisition gradient echo
MRI	Magnetic resonance imaging
MRS	Magnetic resonance spectroscopy
mTBI	Mild traumatic brain injury
MTG	Medial temporal gyrus
NFT	Neurofibrillary tangle
OFC	Orbitofrontal cortex
PCR	Posterior corona radiata
PCT	Pontine crossing tract
PET	Positron emission tomography
PFC	Prefrontal cortex
PIC	Posterior internal capsule
PPV	Positive prediction value
PS	Processing speed
PTR	Posterior thalamic radiation
RIC	Retrolenticular internal capsule
ROI	Region of interest
SCC	Splenium of the corpus callosum
SCbP	Superior cerebellar peduncle
SCR	Superior corona radiata
SFOF	Superior fronto-occipital fasciculus
SLR	Superior longitudinal fasciculus
SS	Sagittal stratum
STG	Superior temporal gyrus
SVM	Support vector machine
SWI	Susceptibility weighted imaging
TBI	Traumatic brain injury
TBSS	Tract-based spatial statistics
TCC	Tapetum of the corpus callosum
TFCE	Threshold-free cluster enhancement
TN	True negative
TNR	True negative rate
TOST	Two one-sided *t* test
TP	True positive
TPR	True positive rate
UF	Uncinate fasciculus
VBM	Voxel-based morphometry
vmPFC	Ventromedial prefrontal cortex
WM	White matter
3D	Three-dimensional

Introduction

In the United States, around 1.7 million individuals incur traumatic brain injuries (TBIs) annually, with an incidence rate of around 500 TBIs per 100,000 people [1]. The Glasgow Coma Scale (GCS) is an assessment tool often used to rate TBI severity using measures of responsiveness like eye-opening and verbal responses [2]. Within the GCS, TBIs can be classified as mild, moderate, or severe based on neurological measures which include loss of consciousness (LOC) duration. In the United States, mild TBI (mTBI) is the most common classification and accounts for ~80% of all TBI cases [1]. Brain morphometry studies of TBI often utilize magnetic resonance imaging (MRI) and computed tomography (CT) [3] to provide noninvasive in vivo mapping, visualization, and quantification of TBI

sequelae. Furthermore, diffusion MRI (dMRI) can be used to quantify the fractional anisotropy (FA) and other properties of water diffusion along white matter (WM) fibers in the TBI-affected brain to identify abnormalities [4].

Chronic TBI effects on cognitive function can share similarities with those of Alzheimer's disease (AD) [5, 6]. Such effects may be particularly severe in older individuals, who are ~3 times more likely to sustain a TBI than those in any other age group [7, 8]. Such greater vulnerability is partly due to a higher risk for physical injuries (like falls) and to a higher likelihood of pre-existing conditions at the time of injury, resulting in poorer clinical outcomes [7]. Repeated mTBIs are particularly associated with AD risk [9–11], and post mortem studies of mTBI effects on brain microstructure have identified both Amyloid β (Aβ) plaques and neurofibrillary tangles (NFTs) of τ protein which resemble those observed in AD [10]. At the macroscale, however, few studies have investigated whether TBI-affected brain structure can change along AD-analogous trajectories, particularly at older ages. Furthermore, the potential relationship between TBI and AD remains underexplored despite the epidemiological significance of both conditions. Independent investigations that used dMRI to compare the FAs of healthy controls (HCs) to those of AD patients and acute mTBI victims found significantly lower FA [4, 12], which is indicative of damage, along WM tracts projecting to the hippocampi and to temporal regions in the brains of AD and mTBI patients [13, 14]. Researchers have also utilized cortical thickness as a measure of gray matter (GM) atrophy and have independently observed similar spatial patterns of cortical thinning in AD and mTBI patients compared to HCs [15–17]. Despite such similarities of findings comparing mTBI and AD to HCs, hardly any studies have combined GM and WM measurements in a longitudinal design to examine whether subacute neurodegeneration after mTBI can occur along AD-analogous trajectories.

Previously, our laboratory showed that the acute cognitive deficits of mTBI patients can predict AD-like chronic alterations in brain *function* with high sensitivity and specificity [18]. To complement these previous findings, the present study leverages MRI-based WM analysis and GM morphometry to compare AD and geriatric mTBI from the standpoint of their observed differences in GM and WM *structure*. The hypothesis of the study is that geriatric mTBI patients are significantly more likely than typically aging adults to exhibit AD-like trajectories of neurodegeneration, even as early as 6 months post injury. This study aims to illustrate our ability to early identify mTBI patients at high risk for AD-analogous neurodegeneration, and to suggest avenues for the early estimation of AD risk after mTBI that may carry substantial potential benefits to medical science.

Methods

This study was conducted with the approval of the Institutional Review Board at the University of Southern California and was carried out in accordance with the Declaration of Helsinki and with the U.S. Code of Federal Regulations (45 C.F.R. 46).

mTBI participants

mTBI participants (N = 33; 15 females; age μ = 62.7 years, σ = 10.6 years, range = 47–83 years) were recruited with the assistance of board-certified clinicians and/or other health professionals who had treated them as outpatients and who had referred them for further neurocognitive assessment, neurological treatment, and/or neuroimaging. The team strove to minimize recruitment bias by inviting all potential participants who satisfied the study's inclusion criteria and who could provide written informed consent. To be included, mTBI volunteers had to have (a) MRI recordings acquired ~6 months post-injury at 3 T, (b) a TBI due to a fall, (c) no clinical findings on acute T_1/T_2-weighted MRI, (d) no clinical findings other than cerebral microbleeds (CMBs) on susceptibility weighted imaging (SWI, an MRI sequence type yielding images on which hemorrhages and other iron-rich brain deposits are hypointense), (e) an acute GCS score greater than 12 (μ = 14.1, σ = 0.7) upon initial medical evaluation, (f) LOC of fewer than 30 min ($\mu \simeq$ 14 min, $\sigma \simeq$ 3 min), (g) post-traumatic amnesia of fewer than 24 h ($\mu \simeq$ 5.5 h, $\sigma \simeq$ 3.2 h), and (h) a lack of clinical history involving pre-traumatic neurological disease or disorders like dementia and mild cognitive impairment (MCI), psychiatric disorder or drug/alcohol abuse. CMBs were identified from SWI, a gradient-echo MRI sequence that is sensitive to the magnetic properties of tissues and fluids such as blood [19]. Specifically, for mTBI subjects, CMBs were first identified manually in each subject by eight human experts with training in neuroimaging and in

CMB identification from SWIs. Consensus meetings to review CMB ratings were then held by a committee including three of the eight experts; each CMB finding was reviewed and discussed thoroughly during these meetings until consensus was reached on the accuracy of each CMB finding. TBI participants' Montréal Cognitive Assessment (MoCA) scores were acquired within 48 h post-injury and ranged between 23 and 30 ($N = 33$, $\mu = 26$, $\sigma = 5$). Mini Mental State Examination (MMSE) scores were also acquired within 48 h post-injury and ranged between 23 and 30 ($N = 33$, $\mu = 25$, $\sigma = 3$). Global Clinical Dementia Rating (CDR) sum of boxes (CDR-SB) scores were not available for TBI participants. No Apolipoprotein E (ApoE) allele information was available for TBI participants.

AD participants

AD patients ($N = 66$; 26 females; age $\mu = 75.6$ y, $\sigma = 8.9$ y, range = 55–92 y) were selected from the AD Neuroimaging Initiative (ADNI) cohort, whose eligibility criteria are described elsewhere [20]. For AD participants, CMBs were identified by a board-certified neurologist. Where available, AD patients' cognitive assessments were made within 0 to 394 days after imaging ($N = 61$, $\mu = 32$ days, $\sigma = 62$ days). AD patients' MoCA scores ranged from 2 to 28 ($N = 61$, $\mu = 15$, $\sigma = 5$), and all had a clinical AD diagnosis. MMSE scores were available for most AD participants ($N = 61$, $\mu = 22$, $\sigma = 3$; range: 11–29). AD patients had global CDR-SB scores between 1 and 14 ($N = 61$, $\mu = 5.35$, $\sigma = 2.34$). For AD patients with ApoE genotyping ($N = 60$), 30% had no $\varepsilon 4$ alleles, 50% had one, and 20% had two.

HC participants

HCs ($N = 81$; 59 females; age $\mu = 68.7$, $\sigma = 7.0$ years, range = 55–87 years) were selected from the ADNI cohort, whose eligibility criteria are described elsewhere [20]. For HC participants, CMBs were identified by a board-certified neurologist. Most HC volunteers' cognitive scores were acquired within 0 to 302 days after imaging ($N = 72$, $\mu = 29$ days, $\sigma = 42$ days). HC participants had been clinically evaluated as having normal cognition; their MoCA scores ranged from 20 to 30 ($N = 72$, $\mu = 26$, $\sigma = 3$). MMSE scores were available for HCs and ranged between 22 and 30 ($N = 72$, $\mu = 29$, $\sigma = 1$). HCs had global CDR-SB scores between 0 and 2 ($N = 72$, $\mu = 0.05$, $\sigma = 0.25$). For HCs whose ApoE genotype had been determined ($N = 68$), the number of ApoE $\varepsilon 4$ alleles was zero for 63% of the sample, one for 34%, and two for 3%.

Data acquisition

HC and AD participant data used for the preparation of this article were obtained from the ADNI database (http://adni.loni.usc.edu). ADNI was launched in 2003 as a public–private partnership, led by Principal Investigator Michael W. Weiner, MD. The primary goal of ADNI has been to test whether serial MRI, positron emission tomography (PET), other biological markers, and clinical and neuropsychological assessment can be combined to measure the progression of MCI and early AD. For up-to-date information, see www.adni-info.org. TBI imaging data were acquired at 3 T using the Prisma MAGNETOM Trio TIM MRI scanner model (20-channel head coil, Siemens Corporation, Erlangen, Germany). Data included T_1- and T_2-weighted, fluid-attenuated inversion recovery (FLAIR), gradient recalled echo (GRE)/SWI, and dMRI volumes. T_1-weighted images were acquired using a three-dimensional (3D), magnetization-prepared rapid acquisition gradient echo (MP-RAGE) sequence [repetition time (T_R) = 1,950 ms; echo time (T_E) = 2.98 ms; inversion time (T_I) = 900 ms; voxel size = 1.0 mm × 1.0 mm × 1.0 mm]. T_2-weighted images were acquired using a 3D sequence ($T_R = 2{,}500$ ms; $T_E = 360$ ms; voxel size = 1.0 mm × 1.0 mm × 1.0 mm) [4]. Flow-compensated GRE/SWI volumes were acquired axially ($T_R = 30$ ms; $T_E = 20$ ms; voxel size = 1.33 mm × 1.33 mm × 1.6 mm). dMRI volumes were acquired axially in 64 gradient directions ($T_R = 8{,}300$ ms; $T_E = 72$ ms; voxel size = 2.7 mm × 2.7 mm × 2 mm). One volume with $b = 0$ s/mm^2 and another with $b = 1{,}000$ s/mm^2 were also acquired, where b is the diffusion-weighting constant of diffusion-weighted imaging (DWI). All acquired data were anonymized and de-linked prior to archiving and analysis.

Preprocessing

DWI volumes were corrected for susceptibility-induced artifacts, subject motion, and eddy currents using software in the FMRIB Software Library (FSL). Based on a pair of images with opposite phase encoding directions, susceptibility-induced artifacts were estimated [21]. Subsequently, a brain mask was created, and

susceptibility corrections were implemented, followed by eddy current and patient motion corrections, resulting in output containing the artifact-corrected, skull-stripped brain volume. Then, the *B* vectors of each volume were rotated such that any inadequate rotations caused by patient motion were accounted for. DWI volumes were further processed in FSL by fitting tensors to corrected DWI volumes to perform diffusion tensor imaging (DTI). These latter volumes were then used for voxel-wise FA calculation such that FA maps could be generated for each volume. T_1-weighted volumes underwent intensity normalization, bias field correction, and motion correction as part of the FreeSurfer 6.0 processing workflow (http://surfer.nmr.mgh.harvard.edu).

Cortical reconstruction

The segmentation of subcortical structures, cerebral WM, and cortical GM was based on T_1-weighted volumes and was implemented in FreeSurfer 6.0 with default execution parameters, as described elsewhere [22, 23]. Briefly, this process includes (1) the removal of non-cerebral voxels using a hybrid watershed/surface deformation procedure, (2) an automated transformation to Talairach space, (3) voxel intensity normalization, (4) segmentation of cortical and subcortical GM, (5) tessellation of the GM/WM boundary, and (6) automated surface topology correction. The reader is referred elsewhere [22, 23] for comprehensive details on each of these steps. Each hemisphere was divided into 74 regions by segmenting subcortical structures and by parceling the cortex into gyri and sulci using the Desikan–Killiany atlas nomenclature [24]. For each subject, cortical thickness was estimated at each cortical location and then resampled onto a seventh-order icosahedral mesh for inter-subject comparison.

Regional labeling and atlasing

WM voxels were mapped onto WM structures in Montreal Neurological Institute (MNI) MNI_{152} space using FSL version 6.0.1 and the Johns Hopkins University (JHU) International Consortium of Brain Mapping (ICBM) DTI_{81} WM labeling scheme. First, the mean FA skeleton mask was co-registered onto the JHU label map, thereby creating a skeletonized version of the latter. Images were then binarized such that voxels corresponding to statistical significance ($p < 0.05$) were set to 1, whereas remaining voxels were set to 0; these binarized images were then projected onto the skeletonized label map. The total number of significant voxels in the volume associated with each label was divided by the total number of voxels pertaining to that label so as to calculate the percentage volume of voxels associated with statistical significance and located in each structure. Results were represented graphically for visual interpretation. For cortical thickness calculations, after binarizing each subject's cortical surface overlay based on statistical significance (1 = significant; 0 = not significant), the resulting binary map was registered onto the average cortical surface in the Desikan–Killiany atlas. Then, a similar procedure was used to calculate the percentage of cortical surface area within each cortical region which contained vertices associated with statistical significance. Figure 1 illustrates a conceptual representation of this process.

Tract-based spatial statistics (TBSS)

A TBSS approach was used for the voxel-wise statistical analysis of mean WM FA differences between groups. In contrast to algorithms involving regions of interest (ROIs) or voxel-based morphometry (VBM) approaches, TBSS utilizes a nonlinear registration algorithm to co-register FA maps, resulting in alignment errors which are substantially smaller than those produced by traditional linear registration algorithms [25]. Moreover, TBSS facilitates the calculation of brain-wide statistics such that both global and local differences in FA can be quantified. First, FA volumes had their end slices set to zero to remove outliers which may have been introduced by fitting diffusion tensors to DWI volume data. After this step, nonlinear transforms to $FMRIB_{58}$ FA standard space were calculated and applied. The $FMRIB_{58}$ FA space was then affinely aligned to the MNI_{152} space and the resulting transform was applied to each subject's FA volume such that all volumes could be aligned to the 1 mm × 1 mm × 1 mm MNI_{152} space. FA maps were then averaged across subjects to generate a mean FA volume which was skeletonized to reveal FA values along the trajectories of major WM structures. The mean FA skeleton was thresholded to remove values below a default threshold of 0.2, below which the low signal-to-noise ratio results in relatively inaccurate FA measurements.

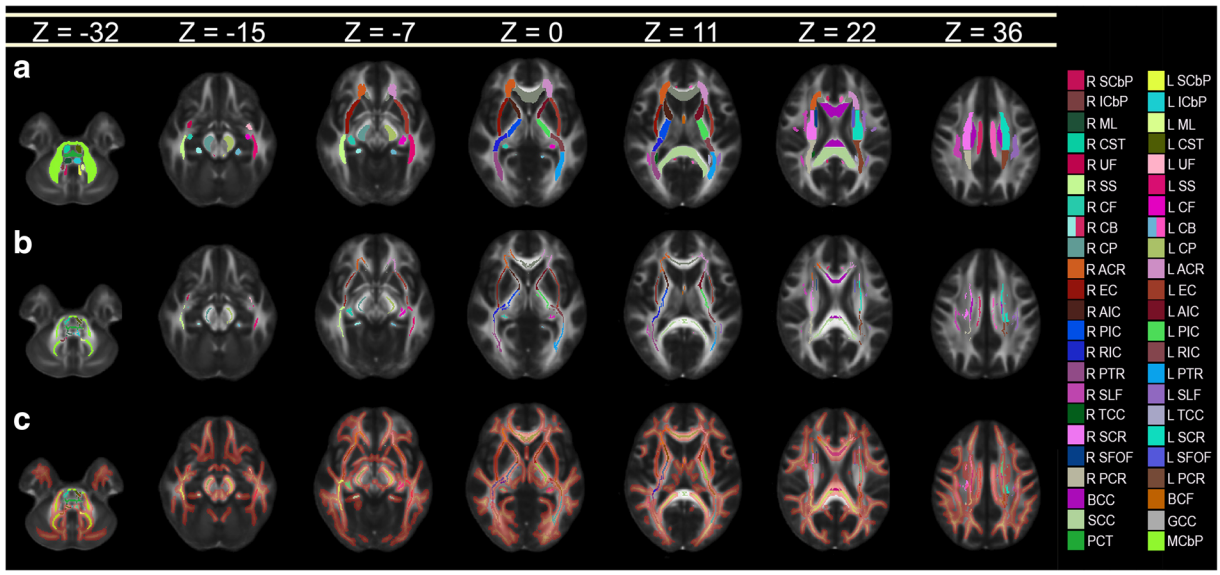

Fig. 1 Conceptual representation of the process for calculating the percentage of voxels associated with statistically significant findings within each neuroanatomic structure. (**a**) WM label map of the JHU atlas. (**b**) Mean WM skeleton mask of all subjects in the study. (**c**) Voxels where mTBI subjects exhibit mean FA values which are significantly lower ($p < 0.05$) than in HCs. The voxel map is overlaid on the skeletonized label map of the atlas, which is thickened for easier visualization. All images are overlaid on the 1 mm × 1 mm × 1 mm $FMRIB_{58}$ FA template, which is an average of FA maps across 58 healthy subjects. Colors encode various WM structures (see Tables 2, 3, and 4 for abbreviations)

Statistical testing of group differences

The statistical significance of differences in age means between the three groups was evaluated using two-tailed Welch's *t* tests. The significance of group differences in sex composition was tested using a χ^2 test. Group differences in mean FA were calculated between (A) AD and mTBI, (B) AD and HCs, and (C) mTBI and HCs. The null hypothesis H_0, according to which each pair of groups' mean FA values are equal, was tested using Welch's *t* test. Using a general linear model (GLM), the confounding effects of sex and age on FA values [26, 27] were regressed out and a nonparametric two-sided *t* test with 500 permutations and with threshold-based free-cluster enhancement (TFCE) was implemented. This revealed clusters of WM voxels whose mean FA differed significantly between groups. All *p* values were corrected for multiple comparisons using 500 nonparametric permutations with TFCE, while controlling for the family-wise error rate (FWER) [28, 29].

Statistical testing of group similarities

A premise of this study is that a brain feature *f* which is both (a) significantly different from HCs in both TBI and AD, *and* (b) significantly similar across TBI and AD, can be said to be *AD-analogous*. Thus, a brain feature *f* observed in TBI patients can be said to be AD-analogous if *f* differs from HCs in both TBI and AD, *and* is also significantly similar across *both* TBI and AD. If *f* differs significantly from HCs in both TBI *and* AD, a null hypothesis of *statistical equivalence* can be tested to determine whether *f* is AD-analogous. Thus, for samples *A* and *B*, a null hypothesis of equivalence is stated as $\mu_A(f) \neq \mu_B(f)$, i.e., as the complement of the typical null hypothesis $\mu_A(f) \neq \mu_B(f)$. A null hypothesis of equivalence fails to be accepted if the two means fall within an interval $(-\delta, +\delta)$, where δ is known as the *equivalence margin* of the test [30]. In a statistical sense, equivalence implies that the values of the empirical estimates of the features $f(A)$ and $f(B)$ are so close that neither estimate can safely be considered to be greater or smaller than the other [31]. In this study, δ is assigned a conservative value equal to 0.2 multiplied by the width of the 95% confidence interval (CI) for the difference $\mu_A(f) - \mu_B(f)$. Equivalence hypotheses were tested using two one-sided *t* tests (TOSTs) [32]. Specifically, the TOSTs were used to quantify the statistical equivalence of FA means between AD and mTBI cohorts. TOSTs are commonly used to test hypotheses of statistical

equivalence [18], which can be interpreted as a measure of statistical similarity between groups.

To identify WM tracts whose FA means were statistically undistinguishable (i.e., statistically equivalent) across mTBI and AD, the null hypothesis H_0 of equivalence was only tested at locations where the mean FA differed significantly from the mean FA for HCs in both the AD and the TBI groups. This restriction was necessary to ensure that any identified statistical equivalences between AD and TBI were associated with deviations from normality (i.e., from HCs). For GM, like for WM, TOSTs were implemented vertex-wise to determine whether the cortical thickness means of the AD and mTBI groups were statistically similar. As in the case of the WM analysis, testing for the statistical equivalence of mean cortical thickness in the AD and mTBI groups was only implemented at locations where each of these groups had been found to differ significantly from HCs. Cortical maps of statistical equivalence between AD and mTBI were generated for display and smoothed across using five iterations of nearest-neighbor interpolation. Equivalence testing was implemented using freely available MATLAB software (https://www.mathworks.com/matlabcentral/fileexchange/63204).

Cognitive impairment vs. brain connectivity alterations

Two support vector machines (SVMs) were designed in MATLAB using the `glmfit`, `fitcsvm`, and `predict` functions with default parameters, the iterative single data algorithm (ISDA), a linear kernel function, and heuristic kernel scale parameters. The SVMs were trained and cross-validated 10-fold to distinguish TBI participants whose AD-like mean FA deviations from normality (i.e., equivalences across TBI and AD) were either relatively *moderate* or relatively *extensive*, respectively. Such deviations were defined as *moderate* or *extensive* depending on whether they belonged to the lowest or highest terciles, respectively, of the TOST statistics' empirical distribution. The number of true negatives (TNs), true positives (TPs), false negatives (FNs), and false positives (FPs) were computed, as were the true positive rate (TPR, or sensitivity), true negative rate (TNR, or specificity), positive prediction value (PPV, or precision), and Matthews' correlation coefficient (MCC) [33].

Results

Participants

Demographics are summarized in Table 1. No significant group differences of sex composition were identified [$\chi^2 = 2.22$, degrees of freedom (df) = 1, $p = 0.136$]. Welch's t test found significant differences in mean age between AD and mTBI (Welch's $t = 6.38$, $df = 97$, $p = 6.31 \times 10^{-4}$), AD and HCs (Welch's $t = 5.28$, $df = 145$, $p = 4.57 \times 10^{-7}$), and mTBI and HCs (Welch's $t = -3.52$, $df = 112$, $p = 6.03 \times 10^{-9}$). CMB counts were found to range from 0 to 2 ($\mu \pm \sigma = 0.27 \pm 0.65$) in HCs, from 0 to 7 ($\mu \pm \sigma = 2.52 \pm 1.91$) in mTBI volunteers, and from 0 to 25 ($\mu \pm \sigma = 1.66 \pm 4.49$) in AD patients. Significant differences in MMSE scores were found between HC and mTBI participants (Welch's $t = -7.49$, $df \simeq 35$, $p = 4.53 \times 10^{-9}$), between HC and AD participants (Welch's $t = 17.01$, $df \simeq 131$, $p < 0.001$) but not between mTBI participants and AD patients (Welch's $t = 4.69$, $df = 64$, $p = 0.99$). Significant differences in MoCA scores were found between HC and AD participants (Welch's $t = 17.26$, $df \simeq 131$, $p = 9.33 \times 10^{-39}$), between acute mTBI participants and AD patients (Welch's $t = 10.65$, $df \simeq 59$, $p = 1.04 \times 10^{-15}$), but not between HC and acute TBI participants (Welch's $t = -0.29$, $df \simeq 42$, $p = 0.39$).

WM comparison between HC and mTBI

Figure 2(a) depicts regions where mTBI subjects had significantly lower mean FA than HCs ($p < 0.05$). In the mTBI group, these regions include the genu and body of the corpus callosum (GCC and BCC, respectively), body and column of the fornix (BCF), as well as crura of the fornix (CF). Table 2 lists WM structures in the descending order of the percentage of voxels within each structure where mean FA is significantly lower in mTBI participants than in HCs. In other words, the percentage of voxels quantifies the proportion of each structure's volume which exhibits significant mean FA differences between the two groups. For example, the first row of Table 2 lists the tapeta of the CC (TCC) and the number 100 in the middle, halfway below the headings labeled "left" and "right." This should be interpreted as indicating that 100% of the TCC spans voxels with statistically significant findings (i.e., the mTBI cohort has significantly lower mean FA values than the HC group across 100% of the TCC). In the

Table 1 Summary of cohort demographics and cognitive assessment data. Dashes indicate data unavailability. Stated are sample sizes (N), mean (μ), standard deviation (σ), minimum value (min), and maximum value (max). Abbreviations: Alzheimer's disease (AD), Clinical Dementia Rating Sum-of-Boxes (CDR-SB), cerebral microbleed (CMB), healthy control (HC), Montreal Cognitive Assessment (MoCA), Mini Mental State Examination (MMSE), traumatic brain injury (TBI), years (yr)

	Age (yr)			MoCA			MMSE			CDR-SB			CMBs		
	HC	TBI	AD	HC	TBI	AD	HC	TBI	AD	HC	TBI	AD	HC	TBI	AD
N	81	33	66	72	33	61	72	33	61	72	—	61	81	32	66
μ	69	63	76	26	26	22	29	25	22	0.05	—	5.35	0.27	1.72	1.66
σ	7	11	9	3	5	3	1	3	3	0.25	—	2.34	0.65	1.67	4.49
min	55	47	55	20	23	2	22	23	11	0	—	1	0	0	0
max	87	83	92	30	30	28	30	30	29	2	—	14	2	7	25

mTBI cohort, the structures whose volumes' mean FAs differ most between groups are the TCC, the uncinate fasciculi (UF), the anterior and posterior internal capsules (AICs and PICs, respectively), the external capsules (ECs), cingulum bundle (CB), superior cerebellar peduncles (SCbPs), BCF, GCC, and BCC. WM structures which (A) are more affected by mTBI in the right hemisphere and which (B) differ to the greatest extent in mTBI compared to HCs include, in descending order, the AIC, SCbP, sagittal stratum (SS), cerebral peduncle (CP), posterior corona radiata (PCR), medial lemniscus (ML), and corticospinal tract (CST). Structures which are more affected in the left hemisphere are the EC, UF, CB, PIC, CF, inferior cerebellar peduncle (ICbP), superior longitudinal fasciculus (SLF), retrolenticular internal capsule (RIC), posterior thalamic radiation (PTR), anterior corona radiata (ACR), superior fronto-occipital fasciculus (SFOF), and superior corona radiata (SCR). No WM fascicles in the mTBI cohort were found to have significantly higher mean FA than in HCs.

WM comparison between HC and AD

Figure 2(b) depicts significant differences in mean FA between the HC and AD cohorts. In AD, mean FA values were significantly lower along commissural fibers like the (A) splenium of the corpus callosum (SCC), the BCC, GCC, BCF, and CF. Table 3 lists WM structures in the descending order of the percentage of each structure's voxels where mean FA is significantly lower in AD participants than in HCs. For example, row 8 of Table 3 lists the SS as well as the numbers 94 and 100 under the "Left" and "Right" headings, respectively. This should be interpreted as indicating that 94% of the left SS and 100% of the right SS span voxels with statistically significant findings (i.e., compared to HCs, the AD cohort has a significantly lower mean FA value in 94% of the left SS and in 100% of the right SS). Thus, compared to HCs, AD patients' mean FAs differ from those of HCs most extensively in the BCC, BCF, CF, UF, CB, GCC, TCC, EC, SS, and SFOF. In descending order according to the same criterion, fasciculi which are more affected in the right hemisphere and which differ most in AD compared to HCs are the CB, TCC, EC, SS, ACR, CP, ML, and PCR. For the left hemisphere, these are the SFOF, PTR, SCbP, AIC, SLF, ICbP, RIC, PIC, SCR, and CST. No WM structures in the AD cohort were found to have significantly greater mean FA than the HC group.

WM comparison between AD and mTBI

No significant differences in mean FA were revealed between the mTBI and AD groups. Equivalence testing comparing mTBI to AD revealed significant statistical similarities of mean FA throughout the brain. Table 4 lists the WM structures in the descending order of the percentage of each structure's voxels for which mean FAs are statistically similar in AD and mTBI participants. For example, the third row in Table 4 lists the pontine crossing tract (PCT) and, halfway between the columns labeled "Left" and "Right," the number 69 is listed. The fact that only one number is listed is due to the fact that there is only one PCT, rather than a "left PCT" or a "right PCT." The numerical entry "69" indicates that 69% of the voxels spanned by the PCT are associated with statistically significant findings (i.e., the AD and mTBI cohorts have significantly similar mean FA values throughout 69% of the PCT). In descending

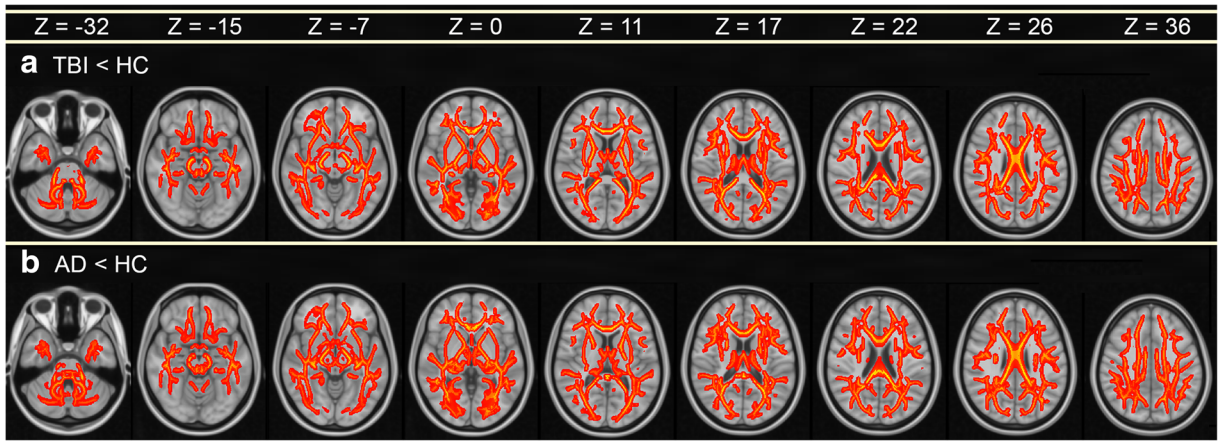

Fig. 2 Statistically significant differences in mean FA between (**a**) HCs and mTBI patients, and between (**b**) HCs and AD patients. Color encodes $-\log_{10} p$, ranging from 2 (red) to 5 (yellow), corresponding to p-values between 0.05 (red) and ~0.0005 (yellow). p values are for t tests using a significance threshold α = 0.05, subject to multiple comparison correction. Smaller p values are associated with higher values of $-\log_{10} p$ and with greater differences in mean FA between the groups compared. Images are displayed in radiologic convention. The z coordinate of each slice in MNI_{152} atlas space is provided

order according to the same criterion, these structures included the SFOF, CF, PCT, ACR, BCF, and SCR.

GM comparison between HC and mTBI

Figure 3(a) displays significant differences in cortical thickness between the HC and mTBI cohorts. In the latter, significantly thinner cortex (blue) is observed in the lateral superior portion of the left temporal lobe, in parietal and in frontal regions. Significantly lower cortical thickness in the HC group (red) is observed diffusely across the cortex. Such cortical thickening after TBI is relatively ubiquitous and has been hypothesized to be associated with chronic inflammation of the GM [17, 34–36].

GM comparison between HC and AD

Figure 3(b) displays significant differences in cortical thickness between the HC and AD cohorts. In the latter, significantly thinner cortex (blue) is found in the lateral and medial parts of the temporal and frontal lobes. In the HC group, significantly thinner cortex (red) is observed at very few locations on the medial surface of the brain, particularly in the cingulate gyri.

GM comparison between mTBI and AD

Figure 3(c) displays regions where cortical thinning was statistically indistinguishable between (i.e., significantly similar across) mTBI and AD cohorts. Extensive areas of statistical similarity are observed in frontotemporal and frontoparietal regions and, more sparsely, in occipital areas. Table 5 lists gyri and sulci in descending order of each structure's percentage (i.e., proportion) of cortical area exhibiting an amount of cortical thinning which was statistically indistinguishable between mTBI and AD. The parcels whose cortical thinning was most statistically similar across mTBI and AD include the superior part of the precentral sulcus, the short insular gyri, the horizontal ramus of the anterior lateral sulcus, the marginal cingulate sulcus, and the orbital gyri. There are few regions whose statistical similarities were largely restricted to a single hemisphere across the AD and mTBI cohorts, including lateral occipital regions, the supramarginal gyri, anterior transverse marginal gyri, inferior parietal lobules, and superior temporal gyri (STG).

Cognitive impairment vs. brain connectivity alterations

Across 100 scenarios, the SVM trained to identify TBI patients whose WM similarities to AD were relatively modest (bottom tercile of equivalence statistic distribution) achieved the following means and standard deviations: TN = 20.0 ± 1.1; TP = 10.0 ± 0.8; FN = 1.6 ± 0.3; FP = 1.4 ± 0.2; TPR = 0.87 ± 0.09; TNR = 0.93 ± 0.09; PPV = 0.88 ± 0.2; MCC = 0.80 ± 0.2. The SVM trained to predict which TBI patients' similarities to AD were relatively extensive (top tercile of equivalence statistic

Table 2 WM structures listed, in descending numerical order, according to the percentage of voxels associated with FA averages which are significantly lower ($p < 0.05$), for each structure, in the mTBI cohort compared to HCs. Values are reported for the left and right hemispheres, except for structures which straddle both; in this latter case, only one value is reported between the left and right hemisphere columns

Abbreviation	Structure	Part	%	
			Left	Right
TCC	Corpus callosum	Tapetum	100	100
EC	External capsule	—	100	99
UF	Uncinate fasciculus	—	100	99
BCC	Corpus callosum	Body	98	
GCC	Corpus callosum	Genu	97	
CB	Cingulum bundle	—	97	96
AIC	Internal capsule	Anterior	94	97
BCF	Fornix	Body	95	
SCbP	Cerebellar peduncle	Superior	91	95
PIC	Internal capsule	Posterior	91	90
SS	Sagittal stratum	—	85	94
CP	Cerebral peduncle	—	87	90
CF	Fornix	Cres	90	87
ICbP	Cerebellar peduncle	Inferior	87	86
SCC	Corpus callosum	Splenium	84	
SLF	Longitudinal fasciculus	Superior	83	82
RIC	Internal capsule	Retrolenticular	92	72
PTR	Thalamic radiation	Posterior	90	74
ACR	Corona radiata	Anterior	83	73
MCbP	Cerebellar peduncle	Middle	78	
SFOF	Fronto-occipital fasciculus	Superior	85	64
PCR	Corona radiata	Posterior	68	79
ML	Medial lemniscus	—	56	68
SCR	Corona radiata	Superior	60	48
CST	Corticospinal tract	—	18	23
PCT	Pontine crossing tract	—	9	

distribution) yielded the following results: TN = 19.2 ± 0.5; TP = 9.1 ± 0.9; FN = 1.1 ± 0.3; FP = 1.9 ± 0.9; TPR = 0.83 ± 0.6; TNR = 0.95 ± 0.5; PPV = 0.83 ± 0.3; MCC = 0.79 ± 0.4.

Discussion

This study investigated cortical thickness and FA changes associated with geriatric mTBI and compared these changes to those observed in AD. The analysis demonstrated (*i*) broad, significant similarities in cortical thinning between mTBI and AD, primarily in the frontal and temporal regions but also in the occipital lobe; (*ii*) bilateral patterns of significant similarities in mean FA across mTBI and AD; and (*iii*) significantly lower mean FA and thinner cortex in both mTBI and AD compared to HCs.

Translational significance

The high prevalence of geriatric mTBI and its subsequent risk for AD underscore the need to predict the latter. Studies have identified significant correlations between certain cognitive measures–like CDR-SB scores—and neural tissue integrity metrics, in that

Table 3 Like Table 2, comparing AD patients to HCs

Abbreviation	Structure	Part	%	
			Left	Right
BCC	Corpus callosum	Body	100	
BCF	Fornix	Body	100	
CF	Fornix	Cres	100	100
UF	Uncinate fasciculus	—	100	100
CB	Cingulum bundle	—	99	100
GCC	Corpus callosum	Genu	99	
TCC	Corpus callosum	Tapetum	97	100
SS	Sagittal stratum	—	94	100
EC	External capsule	—	96	97
SFOF	Fronto-occipital fasciculus	Superior	98	95
PTR	Thalamic radiation	Posterior	99	88
ACR	Corona radiata	Anterior	85	91
SCbP	Cerebellar peduncle	Superior	90	82
SCC	Corpus callosum	Splenium	85	
AIC	Internal capsule	Anterior	93	77
SLF	Longitudinal fasciculus	Superior	88	80
ICbP	Cerebellar peduncle	Inferior	84	79
MCbP	Cerebellar peduncle	Middle	78	
RIC	Internal capsule	Retrolenticular	88	62
CP	Cerebral peduncle	—	73	75
ML	Medial lemniscus	—	72	73
PCR	Corona radiata	Posterior	63	66
PCT	Pontine crossing tract	—	63	
PIC	Internal capsule	Posterior	69	43
SCR	Corona radiata	Superior	54	47
CST	Corticospinal tract	—	15	6

higher CDR-SB scores are indicative of lower integrity [37–39]. Our findings of significant similarities between AD and mTBI pertaining to cortical thickness, mean FA, and cognitive test scores provide clinical insight to identify individuals at high AD risk. Such information can be combined with cognitive test scores (e.g., CDR-SB scores), demographics, biological age prediction [40], and ApoE genotype information to predict the extent and pattern of cortical degeneration experienced by geriatric mTBI patients. Thus, our study may be useful for the stratification of geriatric mTBI patients in terms of their AD risk. Adding to our ability to make such prognostications is the fact that our SVM classification results suggest that the severity of acute cognitive deficits observed in TBI patients can be leveraged *acutely* to predict, with high sensitivities and specificities, the *future* extent and breadth of their AD-like brain atrophy patterns. Such information can also complement information acquired using other functional measures like electroencephalography (EEG) and magnetic resonance spectroscopy (MRS) [41, 42] to gain insights into post-traumatic neuropathophysiology [43–46], including adverse effects of brain injury upon peripheral systems [47–49].

Cognitive testing

Our study features MoCA score ranges of 23–30, 2–28, and 20–30 for mTBI, AD, and HC participants, respectively. MMSE scores range from 23 to 30, 11–29, and

Table 4 WM structures listed, in descending numerical order, according to the percentage of voxels associated with mean FA values which are statistically similar ($p < 0.05$), across mTBI and AD cohorts. Values are reported for the left and right hemispheres, except for structures which straddle both; in this latter case, only one value is reported between the right and left hemisphere columns

Abbreviation	Structure	Part	%	
			Left	Right
SFOF	Fronto-occipital fasciculus	Superior	91	95
CF	Fornix	Cres	65	80
PCT	Pontine crossing tract	—	69	
ACR	Corona radiata	Anterior	58	53
BCF	Fornix	Body	49	
SCR	Corona radiata	Superior	45	52
PTR	Thalamic radiation	Posterior	59	38
PCR	Corona radiata	Posterior	46	45
MCbP	Cerebellar peduncle	Middle	44	
CST	Corticospinal tract	—	36	35
BCC	Corpus callosum	Body	35	
ICbP	Cerebellar peduncle	Inferior	33	33
SLF	Longitudinal fasciculus	Superior	33	27
RIC	Internal capsule	Retrolenticular	28	31
TCC	Corpus callosum	Tapetum	9	43
ML	Medial lemniscus	—	22	30
GCC	Corpus callosum	Genu	23	
CB	Cingulum bundle	—	29	15
SS	Sagittal stratum	—	19	23
SCbP	Cerebellar peduncle	Superior	19	21
PIC	Internal capsule	Posterior	16	23
SCC	Corpus callosum	Splenium	16	
CP	Cerebral peduncle	—	11	13
AIC	Internal capsule	Anterior	13	9
EC	External capsule	—	4	12
UF	Uncinate fasciculus	—	0	7

20–30 for mTBI, AD, and HC subjects, respectively. Typical clinical diagnostic cutoffs for MCI are scores between 18 and 25 for MoCA, and scores between 20 and 25 for MMSE. Although TBI subjects were screened for MCI, it is possible that a minority of subjects had undiagnosed, *subclinical* MCI prior to injury because of MCI prevalence in older individuals [50] and because studying older TBI patients increases the likelihood of including subclinical MCI patients unintentionally [51]. Because both MCI and mTBI are associated with poorer cognition [52], the possibility of including TBI participants with subclinical, premorbid MCI suggests that the sample studied here may have been affected by this condition to a limited extent and that the lower cognitive test scores of some participants could be attributable to both MCI and mTBI.

Structural neurodegeneration in TBI vs. AD

Table 2 lists WM structures with significantly lower average FA values in mTBI patients compared to HCs. The structures with the greatest differences in mean FA include the TCC, EC, UF, BCC, and GCC. Diffuse axonal injury (DAI) accompanies TBI often and commonly affects large WM structures (like the corpus callosum (CC)) as well as fasciculi innervating temporal

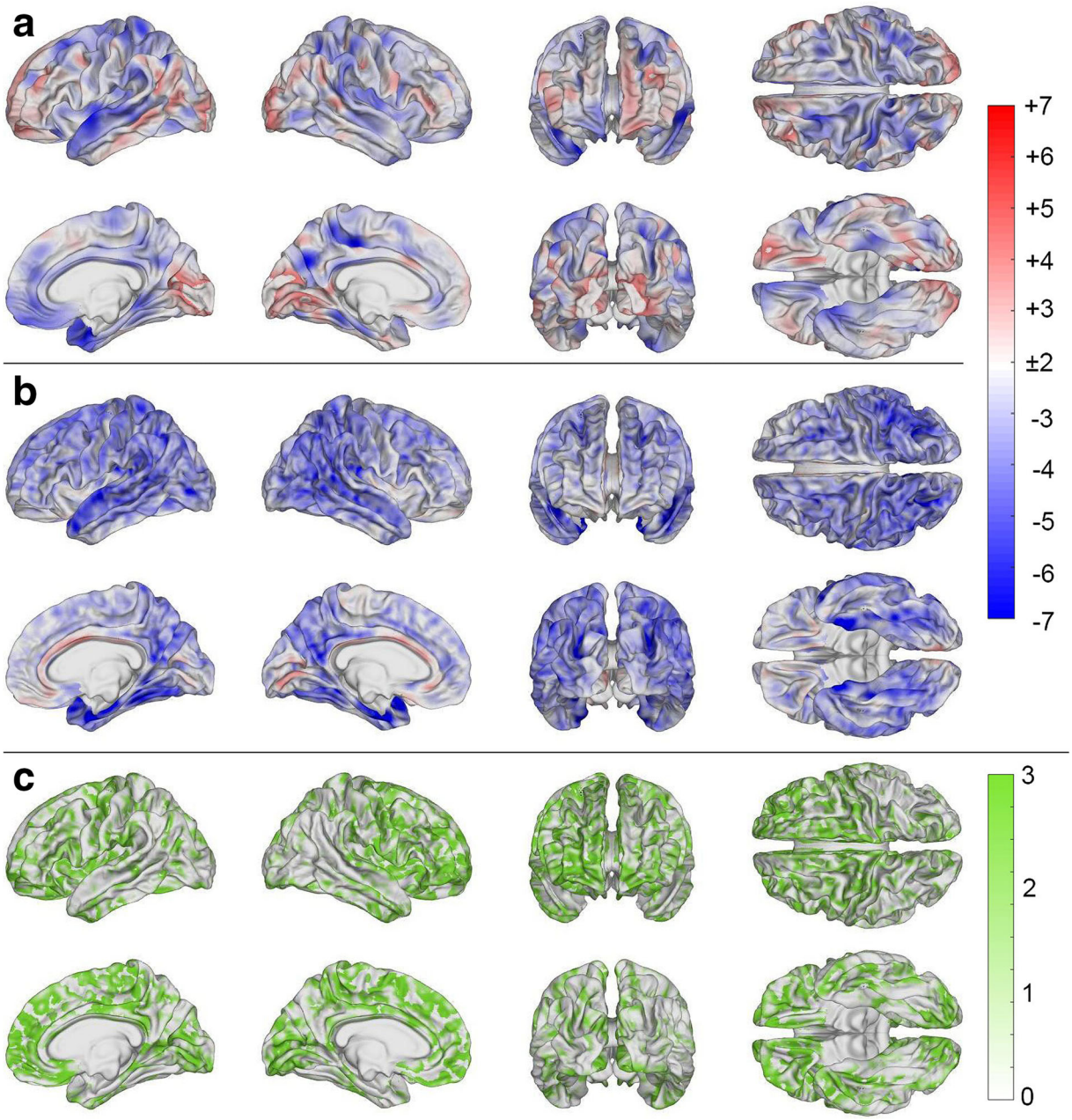

Fig. 3 Statistically significant differences in cortical thickness between (**a**) mTBI and HCs, (**b**) AD and HCs, and (**c**) mTBI and AD patients. Color encodes $-\log_{10} q$, where q is a p value adjusted for the false discovery rate (FDR). Cortical overlays were smoothed using a Gaussian kernel with a full width at half maximum (FWHM) of 5 mm. In (**a**) and (**b**), blue regions represent areas where mTBI and AD subjects, respectively, have significantly thinner cortex compared to HCs. Regions colored in red represent areas where HCs have significantly thinner cortex. In (**c**), areas colored in green represent regions whose mean cortical thickness is statistically indistinguishable across mTBI and AD participants

or frontal regions, like the UF [53–55]. Our findings agree with these previous studies because the UF—which projects to the temporal lobe—is found here to exhibit extensive lower mean FA in mTBI subjects. Structures listed in Table 2 exhibit similar extents of damage across hemispheres; this may be partly attributable to contrecoup injuries that can cause contusions and edema, which affect FA [56]. Thus, the listing of WM

Table 5 GM structures listed, in descending numerical order, according to the percentage of cortical mesh vertices associated with cortical thickness means which are statistically similar ($p < 0.05$), across the mTBI and AD cohorts

Structure	Part/segment	%	
		Left	Right
Part of the precentral sulcus	Superior	91	100
Of the lateral sulcus	Horizontal/anterior	75	86
Short insular gyri	—	71	83
Orbital gyri	—	76	74
Cingulate sulcus	Marginal branch	78	71
Frontomarginal gyrus & sulcus	—	66	79
Insular long gyrus & central sulcus	—	76	64
Of the lateral sulcus	Vertical anterior	72	65
Straight gyrus	—	74	55
Inferior frontal gyrus	Triangular	63	65
Inferior frontal gyrus	Opercular	59	67
Olfactory sulcus	—	57	68
Inferior frontal gyrus	Orbital	55	67
Cingulate gyrus	Posterior/ventral	56	65
Transverse frontopolar gyri & sulci	—	52	69
Subcentral gyrus & sulci	—	65	53
Superior frontal gyrus	—	54	62
Cuneus	—	53	63
Cingulate gyrus & sulcus	Anterior	62	50
Cingulate gyrus & sulcus	Middle/anterior	47	64
Lateral orbital sulcus	—	40	69
Cingulate gyrus & sulcus	Middle/posterior	45	62
Circular sulcus of the insula	Superior	53	49
Inferior temporal gyrus	—	55	47
Paracentral lobule & sulcus	—	58	39
Precentral gyrus	—	34	61
Parieto-occipital sulcus	—	47	47
Inferior frontal sulcus	—	28	66
Lingual gyrus	—	46	47
Middle frontal gyrus	—	35	58
Calcarine sulcus	—	47	44
Subcallosal area & gyrus	—	55	35
Cingulate gyrus	Posterior/dorsal	35	54
Heschl's gyrus	—	54	33
Collateral & lingual sulci	—	31	55
Temporal pole	—	49	36
Central sulcus	—	27	57
Circular sulcus of the insula	Inferior	44	39
Posterior transverse collateral sulcus	—	38	38
Occipital pole	—	37	38
Precuneus	—	35	38
Suborbital sulcus	—	33	37
Superior occipital gyrus	—	39	29
Precentral sulcus	Inferior	32	35
Postcentral gyrus	—	32	32
Supramarginal gyrus	—	36	25
Fusiform gyrus	—	28	32
Inferior occipital gyrus & sulcus	—	31	29
Anterior occipital sulcus	—	23	34
Parahippocampal gyrus	—	28	27
Postcentral sulcus	—	25	29
Middle temporal gyrus	—	24	27
Superior temporal gyrus	Lateral	13	35
Middle frontal sulcus	—	18	29
Anterior transverse collateral sulcus	—	6	39
Superior parietal lobule	—	15	29
Superior & transverse occipital sulci	—	34	9
Superior temporal gyrus	Polar plane	32	11
Circular sulcus of the insula	Anterior	23	19
Orbital sulci	—	17	24
Subparietal sulcus	—	16	20
Middle occipital gyrus	—	19	16
Lateral sulcus	Posterior	16	16
Pericallosal sulcus	—	17	13
Lateral occipito-temporal sulcus	—	18	12
Jensen's sulcus	—	12	13
Superior temporal gyrus	Temporal plane	13	12
Inferior temporal sulcus	—	13	8
Angular gyrus	—	14	1
Superior temporal sulcus	—	0	14
Superior frontal sulcus	—	13	1
Middle occipital & lunati sulci	—	7	4
Intraparietal & transverse parietal sulci	—	3	7

structures in Table 2 is consistent with the set of WM fiber bundles that are commonly reported as being affected by TBI-related DAI.

Table 3 lists the BCC, BCF, CF, UF, and CB as exhibiting significantly lower mean FAs in AD subjects. Two prominent scenarios for AD-related WM degeneration involve Wallerian degeneration and retrogenesis. In Wallerian degeneration, AD-related damage initiated in the GM extends to WM tracts connected to these degenerating GM areas [57]. By contrast, retrogenesis postulates that WM fibers undergoing myelogenesis latest during development are the first to degenerate [58]. Many researchers conceptualize AD neurodegeneration as being due to several competing mechanisms and, thus, as being the product of both phenomena. In Table 3, the structure with the fewest voxels exhibiting lower mean FA in AD is the CST. This agrees with the retrogenesis model, since the CST consists of long, motor-projecting fibers which are among the first to myelinate (and thus among the last to degrade, according to the retrogenesis model). Importantly, our findings of significantly lower mean FA in AD subjects in the BCC, BCF, CF, UF, and CB agree with studies suggesting that frontally- and temporally-projecting fibers are more susceptible to AD neurodegeneration [59–62].

Figures 3(a) and 3(b) depict cortical thinning in the temporal lobes of both mTBI and AD subjects, respectively. Previous studies suggest that such thinning is characteristic of AD and that it precedes the Wallerian degeneration of fibers projecting to these regions. Our study agrees with these findings because Tables 1 and 2 show both mTBI and AD victims as exhibiting significantly lower mean FA than HCs in temporally-projecting fibers like the CB, BCF, and CF. Thus, our findings agree with previous studies of AD-related WM neurodegeneration and may reflect the competing effects of several neurodegenerative mechanisms.

Table 4 illustrates how mTBI and AD are similar from the standpoint of mean FA decreases within major WM fasciculi. Studies have identified WM fibers proximal to the brain stem as being commonly affected by DAI following TBI [55, 63–66]; however, fibers like the PCT and CST are listed here as being relatively spared by both mTBI (Table 2) and AD (Table 3). Instead of appearing to be affected by TBI, these tracts exhibit damage resembling that observed in AD (Table 4). This may reflect similar neurodegeneration mechanisms following TBI and AD [67], and is consistent with the retrogenesis model as these structures are among the first to be myelinated during development [68–70].

Functional neurodegeneration in TBI vs. AD

At the microscale, parallels between TBI and AD have been identified by neuropathology studies [10, 71, 72]. Similarly, in neuropsychological and cognitive studies, neural correlates of cognitive deficits observed after TBI and AD have been found to share commonalities [6, 73]. Nevertheless, few studies have compared the effects of TBI and AD upon brain architecture at the macroscale, partly due to the challenges of MRI morphometry in TBI [74]. The present study found significant similarities between mTBI and AD subjects pertaining to the cortical thinning in the ACC, PCC, and temporal poles (Table 5). Our findings are consistent with those of previous studies [4, 75–78], which independently examined neurodegeneration after the two conditions. Such comparisons of cognitive symptoms across TBI and AD have identified similar deficits in processing speed, cognitive flexibility, attention, and memory [79]. The ACC and PCC are part of the default mode network, which may be hypoactive after mTBI, resulting in deficits of divided attention [80]. Similarly, AD studies of attention suggest that the ACC is involved in divided attention deficits [81]. Simultaneously, TBI-related damage to the ACC and temporal lobes has been implicated in poor self-awareness due to bilateral hyperactivity within these regions. Other studies have found strong involvement of the ACC and temporal poles in functional deficits pertaining to memory and perceptual ability [82, 83]. In what follows, we discuss potential relationships between deficits within specific cognitive domains and both AD- and TBI-related neurodegeneration patterns.

Social function deficits

Social function has been studied in the context of concepts like the *social brain* and the multi-faceted *social network*, which includes the orbitofrontal cortex (OFC), superior aspect of the lateral temporal lobe, the medial prefrontal cortex (PFC), ACC, and the amygdala [84]. The amount of cortical thinning identified by our investigation in the OFC was found to be statistically indistinguishable across the mTBI and AD cohorts (Table 5), which is consistent with studies identifying the OFC as modulating social function. Specifically, in TBI, the OFC has been cited as involved in social function (e.g., emotion recognition), and prominent mTBI-

related deficits pertain to social function [85–87]. This type of deficit has also been identified in AD, where social withdrawal and dysfunction are typical manifestations of the disease [84, 88, 89]. Thus, our findings suggest that TBI and AD share social function deficits which may be due to similar spatial neurodegeneration patterns.

Decision-making deficits

This study found that damage to the PIC, UF, orbital gyri, and orbital sulci is common in both mTBI and AD (Tables 3 and 4). Typically, decision-making after TBI is significantly poorer than in HCs, a phenomenon which often persists up to 5 years post injury [90]. There are, however, conflicting findings on how lesion location impacts decision-making. In mice, for example, spatially non-specific associations have been found between unilateral parietal and bilateral frontal lesions, on the one hand, and riskier decision-making and increased impulsivity, on the other hand [91, 92]. By contrast, however, human studies indicate that decision-making deficits are not limited to cases involving frontal lesions [93]. Thus, dMRI studies of patients with mild-to-moderate blast TBIs have revealed that the compromised integrities of the right UF, right inferior fronto-occipital fasciculus (IFOF), and right PIC are associated with decision-making deficits [94]. Aside from TBI, such deficits are also observed in AD, where structural changes within ventromedial PFC (vmPFC) are correlated with measurable deficits [95]. Thus, our findings are consistent with those of prior studies on decision-making and identify commonalities between decision making deficits and the neurodegenerative patterns of TBI and AD.

PS deficits

This study identified similar patterns of WM degradation across mTBI and AD in the left AIC, UF, CB, ACR, and GCC (Table 4). Such findings are consistent with those of previous dMRI studies that revealed correlations between reduced WM integrity in these areas and relatively low PS [96–99]. In mTBI, lower PS has been reported as early as 1-month post-injury and has been documented to persist for up to 6 years post-injury [100–103]. Commonly, lower PS is coexistent with other mTBI-related symptoms like fatigue, anxiety, and attention deficits. In particular, reports of fatigue following mTBI are exceedingly common and may be explained by the *coping hypothesis*, which states that compensatory recruitment of areas increases cognitive load, resulting in fatigue which lowers PS [104–107]. Similar PS reductions have been observed in AD, as quantified by pause and reaction times [108, 109]. Thus, our findings agree with those of previous studies which identified neuroanatomic structure correlates of PS deficits in TBI and AD.

Verbal fluency deficits

Our study reports similarities between mTBI and AD pertaining to global reductions in cortical thickness (Table 5). Some of these affected structures and regions (e.g., the left ascending fibers in the CC, the frontal lobes, the left inferior frontal gyrus (IFG), the left middle temporal gyrus (MTG), and the left STG have been identified as being responsible for reduced verbal fluency [110–112]. Verbal fluency can be broadly classified as phonemic or semantic, and deficits in both are frequent after TBI, with estimated prevalences of ~70% and ~87%, respectively, and with comparable magnitudes for each [113, 114]. Whereas other deficits following TBI can recover relatively well, verbal fluency deficits have been suggested to recover relatively poorly and slowly, since they persist for more than 6 weeks post-injury [115, 116]. In AD, deficits in both phonemic and semantic fluency have been observed. Importantly, the latter is reported as being significantly more impaired than the former [117]. Such differences in severity have been proposed to reflect the increased susceptibility of temporal regions—which have a role in semantic memory—to neurodegeneration following AD [118, 119]. Figure 2b displays reduced cortical thickness in the temporal regions of AD subjects, in agreement with previous studies [16, 120]. Thus, the degradation of brain regions reported here is consistent with the findings of previous studies reporting relatively slow recovery of verbal fluency after TBI. Together, our findings indicate that TBI and AD share neuroanatomic patterns of brain degradation which underlie verbal fluency deficits.

Executive function (EF) deficits

EF is greatly impacted by both mTBI and AD [121–124]. Here we identified relatively low mean FA in the ACCs, GCCs, SCCs, and PICs of both mTBI and

AD patients compared to HCs (Tables 1 and 2). Reduced integrity in these WM structures is correlated with impaired planning abilities [81, 125], although such findings are not unanimous across studies [126]. This may suggest that planning deficits are modulated by injury severity, particularly since some authors [127] did not identify planning deficits associated with WM damage. By contrast, AD patients' planning deficits have been documented extensively and there is substantial consensus on their profiles [81, 128–130]. Thus, our findings of similarly reduced WM integrity in the CCs of mTBI and AD subjects are consistent with previous studies tying these areas to EF deficits [131, 132].

Cognitive flexibility deficits

Reductions in cognitive flexibility are often noted after mTBI and have been documented both acutely and up to 2 months after injury. Our study revealed reduced WM integrity throughout the CCs of mTBI and AD patients, in agreement with investigations of these areas' involvement in EF. Inflexibility affects multiple facets of cognition, including the ability to integrate new information, to adapt one's behavior in response to stimuli, and to switch attention fluidly. Cognitive flexibility is intimately related to EF, which recruits frontal cortex and frontally-projecting fibers [122]. Because of this, similar methods like task switching have been used to reveal that reduced GM integrity–particularly in the superior frontal gyrus (SFG), PFC, precuneus, ACC, and in the fusiform gyrus–affects cognitive flexibility [133, 134]. In our mTBI and AD cohorts, reduced cortical thickness was observed in the superior FG, in the PFC, precuneus, ACC, and in the fusiform gyrus (Table 5). Thus, our findings support the hypothesis according to which AD and TBI patients share a previously documented neuroanatomic substrate of cognitive inflexibility.

Limitations

Although the results of this study support an association between mTBI and AD, it is imperative that they be interpreted cautiously because they do not establish a causal relationship between TBI and AD. Specifically, because the associations reported here pertaining to the relationship between mTBI and brain structure are of a statistical nature, it is important to keep in mind that these statistical relationships may not be causally linked solely to TBI. Rather, our findings support the hypothesis that, to some extent, mTBI and AD share some commonality of trajectories. Furthermore, because the participant follow-up period is limited to the first ~6 months post-injury, our findings do not reflect the entire range of TBI progression, nor do they establish whether and when neurodegeneration trajectories diverge across the two conditions. To establish such cause–effect relationships between mTBI and AD, more definitive and larger prospective studies should evaluate, within a broader longitudinal design, the cerebral structure of geriatric mTBI victims. Thus, the possibility that our findings may in part be due to conditions other than TBI cannot be discarded and is, in fact, plausible. For example, it is important to acknowledge that comorbidities may influence the structural findings reported here. For example, in one UK study of geriatric TBI involving hospital admissions [135], 11% of patients had pre-existing dementia, 22% had pre-existing hypertension, and 99% had at least one pre-existing medical condition. Similarly, Mosenthal et al. [136] report that 73% of older TBI patients have a medical condition before injury, compared with only 28% of younger adults. Third, 80% of all adults aged 65 years and older have at least one chronic condition and 50% have at least two [137]. Thus, typically, older TBI patients suffer from at least one cardiovascular comorbidity, like hypertension. Pre-existing hypertension is common in geriatric TBI patients [138] and its association with lower FA compared to normotensive patients [139] may be due to the adverse effects of hypertension upon the neurovasculature. CMBs—whose presence can result in mean FA decreases [140]—are common in geriatric TBI and can significantly affect peri-hemorrhagic WM [4]. CMBs are also frequent in cases of cerebral amyloid angiopathy (CAA), which is a risk factor for AD [141, 142]. Thus, due to the high prevalence of CMB-positive TBI comorbidities in older adults, it is possible that our findings of structural similarities between mTBI and AD are partially due to pre-existing neurovascular conditions. Thus, ideally, the structural effects of AD and mTBI should be compared in the absence of CMBs, which may confound findings. However, this may be challenging due to the high prevalence of vascular disease in older adults; furthermore, findings from such normotensive older TBI patients who are free of vascular disease may be of somewhat limited applicability to

most clinical settings because only a relatively modest cross-section of older individuals lack either symptoms or post-mortem pathology indicative of vascular disease. Finally, it should be noted that CMB counts, although reported here, were not included in our analysis of WM degradation because accounting for local CMB effects is challenging and outside the scope of this study. The reader is referred to our previous research for findings on this topic [4].

The possibility of unintentional sampling bias is another study limitation that should be acknowledged. Thus, although random sampling from the entire TBI population—or at least from the local TBI population—would have been preferable, such sampling was logistically unfeasible for us as no comprehensive directory of geriatric TBI victims was available to us at the time of the study. Instead, our most viable option was reaching out to potential volunteers based on referrals from clinicians.

One technical limitation of this study is that the JHU WM atlas includes only 25 WM structures and omits some functionally prominent fascicles. For example, superficial WM streamlines—described as typically short cortical association fibers near the surface of the cortex [143]—are excluded here. Such connections are more difficult to segment and more poorly documented than larger WM structures, and since the JHU WM atlas does not include them, neither does our study. Future studies should use atlases that map more WM structures; in our case, this was beyond the scope of the study as our primary interest was in the largest and best-mapped WM structures in the brain. Another limitation is the fact that MRI data used in the study were acquired at distinct sites using different scanners. This is known to confound measurements of both cortical thickness and WM properties [144, 145], such that harmonization protocols like ComBat can be useful [144–146]. Nevertheless, because our MRI acquisition protocol parameters were very similar across sites and scanners, such confounds may not be substantial in this study.

Although age-related effects were regressed out in our statistical analyses, the groups included here did exhibit significant mean differences of age. These differences are partly due to our selection of subjects from retrospective samples of convenience, such that age matching across groups was possible to a very limited extent. Furthermore, because this is a longitudinal study involving both structural MRI and dMRI of individuals with very specific eligibility criteria, only a relatively small subsample of the ADNI cohort was useful for our purposes. This also limited our ability to match subjects by age. Finally, AD occurs relatively rarely before the age of 65, whereas TBIs can occur at any age. This implies that comparing AD patients to TBI victims can be problematic if the latter are relatively young compared to the former. Thus, to some extent, the confound of age in studies like ours is unavoidable if young or middle-aged TBI patients are to be compared to AD patients. Nevertheless, because TBI patients younger than 65 may still be vulnerable to AD-analogous neurodegeneration (as suggested, in fact, by our study), the inability to match TBI and AD patients by age may be unavoidable in studies like ours, particularly if relatively young TBI patients are studied.

Conclusion

Upon comparing AD patients to mTBI participants imaged ~6 months post injury, this study identified statistical similarities between these groups pertaining to both WM and GM neurodegeneration, as evidenced by both mean FA and cortical thickness measurements. Whereas other studies explored the effects of TBI and AD on the brain without reference to one another, we directly compare such effects. Furthermore, this study focuses on chronic mTBI findings rather than on acute mTBI, thereby providing insight into the medium-to-long-term effects of mTBI upon macroscale brain structure. Our findings agree with those of previous studies of functional and structural correlates in these conditions, and additionally reveal AD-analogous patterns of neurodegeneration after mTBI, which may be proportional to AD risk. Thus, our findings are relevant to ongoing efforts to identify mTBI patients at high risk for AD. Future studies should quantitatively compare the neurological and neuropsychological consequences of mTBI and AD to further elucidate their relationship.

Acknowledgements The authors thank Sean Mahoney, Van Ngo, and Di Fan for suggestions and comments on the manuscript, Nikhil N. Chaudhari for assistance with CMB identification, data archiving, and data retrieval, as well as Nahian F. Chowdhury, Gloria Chia-Yi Chiang, Ammar Dharani, Jun H. Kim, Hyung Jun Lee, David J. Robles, and Shania H. Wang for assistance with CMB identification. Data used in preparation of this article were obtained from the Alzheimer's Disease Neuroimaging Initiative

(ADNI) database (adni.loni.usc.edu). As such, the investigators within the ADNI contributed to the design and implementation of ADNI and/or provided data but did not participate in analysis or writing of this report. A complete listing of ADNI investigators can be found at: http://adni.loni.usc.edu/wp-content/uploads/how_to_apply/ADNI_Acknowledge-ment_List.pdf.

Availability of data and material MRI data acquired from HC and AD participants are publicly available from the ADNI database (http://adni.loni.usc.edu). For TBI participants, primary data generated during and/or analyzed during the current study are available subject to a data transfer agreement. At the request of some participants, their written permission is additionally required in some cases.

Code availability The computer code used in this study is freely available. FreeSurfer (https://surfer.nmr.mgh.harvard.edu) and the FMRIB Software Library (https://fsl.fmrib.ox.ac.uk) are freely available. Equivalence testing was implemented using freely available MATLAB software (https://www.mathworks.com/matlabcentral/fileexchange/63204). Regression and SVM analyses were implemented in MATLAB (http://mathworks.com) using the `glmfit`, `fitcsvm`, and `predict` functions.

Author contribution K.A.R. and A.I. contributed to the study design, data analysis, result interpretation, and manuscript redaction.

Funding This work was supported by NIH grant R01 NS 100973 to A.I., by DoD award W81-XWH-1810413 to A.I., by a Hanson-Thorell Research Scholarship to A.I., and by a grant from the Undergraduate Research Associate Program (URAP) at the University of Southern California to A.I. Data collection and sharing for this project were funded by the Alzheimer's Disease Neuroimaging Initiative (ADNI, NIH Grant U01 AG024904) and DoD ADNI (DoD award number W81XWH-12-2-0012). ADNI is funded by the National Institute on Aging, the National Institute of Biomedical Imaging and Bioengineering, and through generous contributions from the following: AbbVie, Alzheimer's Association; Alzheimer's Drug Discovery Foundation; Araclon Biotech; BioClinica, Inc.; Biogen; Bristol-Myers Squibb Company; CereSpir, Inc.; Cogstate; Eisai Inc.; Elan Pharmaceuticals, Inc.; Eli Lilly and Company; EuroImmun; F. Hoffmann-La Roche Ltd, and its affiliated company Genentech, Inc.; Fujirebio; GE Healthcare; IXICO Ltd.; Janssen Alzheimer Immunotherapy Research & Development, LLC.; Johnson & Johnson Pharmaceutical Research & Development LLC.; Lumosity; Lundbeck; Merck & Co., Inc.; Meso Scale Diagnostics, LLC.; NeuroRx Research; Neurotrack Technologies; Novartis Pharmaceuticals Corporation; Pfizer Inc.; Piramal Imaging; Servier; Takeda Pharmaceutical Company; and Transition Therapeutics. The Canadian Institutes of Health Research is providing funds to support ADNI clinical sites in Canada. Private sector contributions are facilitated by the Foundation for the National Institutes of Health (www.fnih.org). The grantee organization is the Northern California Institute for Research and Education, and the study is coordinated by the Alzheimer's Therapeutic Research Institute at the University of Southern California. ADNI data are disseminated by the Laboratory for Neuro Imaging at the University of Southern California.

Declarations

Ethics approval This study was conducted with the approval of the Institutional Review Board at the University of Southern California and was carried out in accordance with the Declaration of Helsinki and with the U.S. Code of Federal Regulations (45 C.F.R. 46).

Consent to participate All subjects provided written informed consent.

Consent for publication Both authors approved the final version of the manuscript for publication.

Conflict of interest/Competing interests The authors declare that this research was conducted with no commercial or financial relationships that could be construed as a potential conflict of interest statement.

References

1. Georges A, Booker JG. Traumatic Brain Injury. Treasure Island (FL): StatPearls; 2020.
2. Jain S, Iverson LM. Glasgow Coma Scale. Treasure Island (FL): StatPearls; 2020.
3. Irimia A, Maher AS, Rostowsky KA, Chowdhury NF, Hwang DH, Law EM. Brain segmentation from computed tomography of healthy aging and geriatric concussion at variable spatial resolutions. Front Neuroinform. 2019;13:9. https://doi.org/10.3389/fninf.2019.00009.
4. Rostowsky KA, Maher AS, Irimia A. Macroscale white matter alterations due to traumatic cerebral microhemorrhages are revealed by diffusion tensor imaging. Front Neurol. 2018;9:948. https://doi.org/10.3389/fneur.2018.00948.
5. Moretti L, Cristofori I, Weaver SM, Chau A, Portelli JN, Grafman J. Cognitive decline in older adults with a history of traumatic brain injury. Lancet Neurol. 2012;11(12):1103–12. https://doi.org/10.1016/S1474-4422(12)70226-0.
6. Kinnunen KM, Greenwood R, Powell JH, Leech R, Hawkins PC, Bonnelle V, et al. White matter damage and cognitive impairment after traumatic brain injury. Brain. 2011;134(Pt 2):449–63. https://doi.org/10.1093/brain/awq347.
7. Thompson HJ, McCormick WC, Kagan SH. Traumatic brain injury in older adults: epidemiology, outcomes, and future implications. J Am Geriatr Soc. 2006;54(10):1590–5. https://doi.org/10.1111/j.1532-5415.2006.00894.x.
8. LeBlanc J, de Guise E, Gosselin N, Feyz M. Comparison of functional outcome following acute care in young, middle-aged and elderly patients with traumatic brain injury. Brain Inj. 2006;20(8):779–90. https://doi.org/10.1080/02699050600831835.

9. Li Y, Li Y, Li X, Zhang S, Zhao J, Zhu X, et al. Head Injury as a risk factor for dementia and Alzheimer's Disease: a systematic review and meta-analysis of 32 observational studies. PLoS One. 2017;12(1):e0169650. https://doi.org/10.1371/journal.pone.0169650.
10. Washington PM, Villapol S, Burns MP. Polypathology and dementia after brain trauma: does brain injury trigger distinct neurodegenerative diseases, or should they be classified together as traumatic encephalopathy? Exp Neurol. 2016;275(Pt 3):381–8. https://doi.org/10.1016/j.expneurol.2015.06.015.
11. Edwards G 3rd, Moreno-Gonzalez I, Soto C. Amyloid-beta and tau pathology following repetitive mild traumatic brain injury. Biochem Biophys Res Commun. 2017;483(4):1137–42. https://doi.org/10.1016/j.bbrc.2016.07.123.
12. Irimia A, Fan D, Chaudhari N, Ngo V, Zhang F, Joshi SH, et al. Mapping cerebral connectivity changes after mild traumatic brain injury in older adults using diffusion tensor imaging and Riemannian matching of elastic curves. In: Conference Proceedings of the 17th IEEE International Symposium on Biomedical Imaging. Iowa City, IA, USA: IEEE; 2020. p. 1690-1693.
13. Chen SQ, Kang Z, Hu XQ, Hu B, Zou Y. Diffusion tensor imaging of the brain in patients with Alzheimer's disease and cerebrovascular lesions. J Zhejiang Univ Sci B. 2007;8(4):242–7. https://doi.org/10.1631/jzus.2007.B0242.
14. Davenport ND, Lim KO, Armstrong MT, Sponheim SR. Diffuse and spatially variable white matter disruptions are associated with blast-related mild traumatic brain injury. Neuroimage. 2012;59(3):2017–24. https://doi.org/10.1016/j.neuroimage.2011.10.050.
15. Santhanam P, Wilson SH, Oakes TR, Weaver LK. Accelerated age-related cortical thinning in mild traumatic brain injury. Brain Behav. 2019;9(1):e01161. https://doi.org/10.1002/brb3.1161.
16. Du AT, Schuff N, Kramer JH, Rosen HJ, Gorno-Tempini ML, Rankin K, et al. Different regional patterns of cortical thinning in Alzheimer's disease and frontotemporal dementia. Brain. 2007;130(Pt 4):1159–66. https://doi.org/10.1093/brain/awm016.
17. Govindarajan KA, Narayana PA, Hasan KM, Wilde EA, Levin HS, Hunter JV, et al. Cortical thickness in mild traumatic brain injury. J Neurotrauma. 2016;33(20):1809–17. https://doi.org/10.1089/neu.2015.4253.
18. Irimia A, Maher AS, Chaudhari NN, Chowdhury NF, Jacobs EB. Acute cognitive deficits after traumatic brain injury predict Alzheimer's disease-like degradation of the human default mode network. Geroscience. 2020;42(5):1411-1429. doi:https://doi.org/10.1007/s11357-020-00245-6
19. Sehgal V, Delproposto Z, Haacke EM, Tong KA, Wycliffe N, Kido DK, et al. Clinical applications of neuroimaging with susceptibility-weighted imaging. J Magn Reson Imaging. 2005;22(4):439–50. https://doi.org/10.1002/jmri.20404.
20. Petersen RC, Aisen PS, Beckett LA, Donohue MC, Gamst AC, Harvey DJ, et al. Alzheimer's Disease Neuroimaging Initiative (ADNI): clinical characterization. Neurology. 2010;74(3):201–9. https://doi.org/10.1212/WNL.0b013e3181cb3e25.
21. Andersson JL, Skare S, Ashburner J. How to correct susceptibility distortions in spin-echo echo-planar images: application to diffusion tensor imaging. Neuroimage. 2003;20(2):870–88. https://doi.org/10.1016/S1053-8119(03)00336-7.
22. Dale AM, Fischl B, Sereno MI. Cortical surface-based analysis. I. Segmentation and surface reconstruction. Neuroimage. 1999;9(2):179–94. https://doi.org/10.1006/nimg.1998.0395.
23. Fischl B, Sereno MI, Dale AM. Cortical surface-based analysis. II: inflation, flattening, and a surface-based coordinate system. Neuroimage. 1999;9(2):195–207. https://doi.org/10.1006/nimg.1998.0396.
24. Desikan RS, Segonne F, Fischl B, Quinn BT, Dickerson BC, Blacker D, et al. An automated labeling system for subdividing the human cerebral cortex on MRI scans into gyral based regions of interest. Neuroimage. 2006;31(3):968–80. https://doi.org/10.1016/j.neuroimage.2006.01.021.
25. Smith SM, Jenkinson M, Johansen-Berg H, Rueckert D, Nichols TE, Mackay CE, et al. Tract-based spatial statistics: voxelwise analysis of multi-subject diffusion data. Neuroimage. 2006;31(4):1487–505. https://doi.org/10.1016/j.neuroimage.2006.02.024.
26. Bennett IJ, Madden DJ, Vaidya CJ, Howard DV, Howard JH Jr. Age-related differences in multiple measures of white matter integrity: a diffusion tensor imaging study of healthy aging. Hum Brain Mapp. 2010;31(3):378–90. https://doi.org/10.1002/hbm.20872.
27. Kanaan RA, Allin M, Picchioni M, Barker GJ, Daly E, Shergill SS, et al. Gender differences in white matter microstructure. PLoS One. 2012;7(6):e38272. https://doi.org/10.1371/journal.pone.0038272.
28. Smith SM, Nichols TE. Threshold-free cluster enhancement: addressing problems of smoothing, threshold dependence and localisation in cluster inference. Neuroimage. 2009;44(1):83–98. https://doi.org/10.1016/j.neuroimage.2008.03.061.
29. Han H, Glenn AL, Dawson KJ. Evaluating alternative correction methods for multiple comparison in functional neuroimaging research. Brain Sci. 2019;9:8. https://doi.org/10.3390/brainsci9080198.
30. Wellek S. A new approach to equivalence assessment in standard comparative bioavailability trials by means of the Mann-Whitney statistic. Biometrical Journal. 1996;38(6):695–710. https://doi.org/10.1002/bimj.4710380608.
31. Walker E, Nowacki AS. Understanding equivalence and noninferiority testing. Journal of General Internal Medicine. 2011;26(2):192–6. https://doi.org/10.1007/s11606-010-1513-8.
32. Hoffelder T, Gossl R, Wellek S. Multivariate equivalence tests for use in pharmaceutical development. Journal of Biopharmaceutical Statistics. 2015;25(3):417–37. https://doi.org/10.1080/10543406.2014.920344.
33. Matthews BW. Comparison of the predicted and observed secondary structure of T4 phage lysozyme. Biochim Biophys Acta. 1975;405(2):442–51. https://doi.org/10.1016/0005-2795(75)90109-9.
34. Dall'Acqua P, Johannes S, Mica L, Simmen H-P, Glaab R, Fandino J, et al. Prefrontal cortical thickening after mild traumatic brain injury: a one-year magnetic resonance

imaging study. Journal of Neurotrauma. 2017a;34(23):3270–9. https://doi.org/10.1089/neu.2017.5124.
35. Guerriero RM, Giza CC, Rotenberg A. Glutamate and GABA imbalance following traumatic brain injury. Curr Neurol Neurosci Rep. 2015;15(5):27. https://doi.org/10.1007/s11910-015-0545-1.
36. Shao M, Cao J, Bai L, Huang W, Wang S, Sun C, et al. Preliminary evidence of sex differences in cortical thickness following acute mild traumatic brain injury. Front Neurol. 2018;9:878. https://doi.org/10.3389/fneur.2018.00878.
37. Ji F, Pasternak O, Liu S, Loke YM, Choo BL, Hilal S, et al. Distinct white matter microstructural abnormalities and extracellular water increases relate to cognitive impairment in Alzheimer's disease with and without cerebrovascular disease. Alzheimers Res Ther. 2017;9(1):63. https://doi.org/10.1186/s13195-017-0292-4.
38. Hsu JL, Lee WJ, Liao YC, Lirng JF, Wang SJ, Fuh JL. Posterior atrophy and medial temporal atrophy scores are associated with different symptoms in patients with Alzheimer's disease and mild cognitive impairment. PLoS One. 2015;10(9):e0137121. https://doi.org/10.1371/journal.pone.0137121.
39. Wang B, Prastawa M, Awate SP, Irimia A, Chambers MC, Vespa PM, et al. Segmentation of serial MRIs of TBI patients using personalized atlas construction and topological change estimation. Proc IEEE Int Symp Biomed Imaging. 2012:1152–5. https://doi.org/10.1109/isbi.2012.6235764.
40. Irimia A, Torgerson CM, Goh SY, Van Horn JD. Statistical estimation of physiological brain age as a descriptor of senescence rate during adulthood. Brain Imaging Behav. 2015;9(4):678–89. https://doi.org/10.1007/s11682-014-9321-0.
41. Van Horn JD, Bhattrai A, Irimia A. Multimodal imaging of neurometabolic pathology due to traumatic brain injury. Trends in Neurosciences. 2017;40(1):39–59. https://doi.org/10.1016/j.tins.2016.10.007.
42. Halgren E, Sherfey J, Irimia A, Dale AM, Marinkovic K. Sequential temporo-fronto-temporal activation during monitoring of the auditory environment for temporal patterns. Hum Brain Mapp. 2011;32(8):1260–76. https://doi.org/10.1002/hbm.21106.
43. Irimia A, Van Horn JD. Functional neuroimaging of traumatic brain injury: advances and clinical utility. Neuropsychiatr Dis Treat. 2015;11:2355–65. https://doi.org/10.2147/NDT.S79174.
44. Irimia A, Van Horn JD. Epileptogenic focus localization in treatment-resistant post-traumatic epilepsy. Journal of Clinical Neuroscience. 2015;22(4):627–31.
45. Lima EA, Irimia A, Wikswo J. The magnetic inverse problem. In: Braginski AI, Clarke J, editors. The SQUID Handbook. Weinheim, Germany: Wiley-VCH; 2006. p. 139–267.
46. Irimia A, Goh SY, Torgerson CM, Chambers MC, Kikinis R, Van Horn JD. Forward and inverse electroencephalographic modeling in health and in acute traumatic brain injury. Clinical Neurophysiology. 2013;124(11):2129–45.
47. Irimia A, Bradshaw LA. Ellipsoidal electrogastrographic forward modelling. Phys Med Biol. 2005;50(18):4429–44. https://doi.org/10.1088/0031-9155/50/18/012.
48. Irimia A, Richards WO, Bradshaw LA. Magnetogastrographic detection of gastric electrical response activity in humans. Phys Med Biol. 2006;51(5):1347–60. https://doi.org/10.1088/0031-9155/51/5/022.
49. Irimia A. Electric field and potential calculation for a bioelectric current dipole in an ellipsoidl. Journal of Physics A: Mathematical and General. 2005;38(37):8123–38.
50. Eshkoor SA, Hamid TA, Mun CY, Ng CK. Mild cognitive impairment and its management in older people. Clin Interv Aging. 2015;10:687–93. https://doi.org/10.2147/CIA.S73922.
51. Sachdev PS, Lipnicki DM, Kochan NA, Crawford JD, Thalamuthu A, Andrews G, et al. The prevalence of mild cognitive impairment in diverse geographical and ethnocultural regions: The COSMIC Collaboration. PLoS One. 2015;10(11):e0142388. https://doi.org/10.1371/journal.pone.0142388.
52. de Freitas Cardoso MG, Faleiro RM, de Paula JJ, Kummer A, Caramelli P, Teixeira AL, et al. Cognitive impairment following acute mild traumatic brain injury. Front Neurol. 2019;10:198. https://doi.org/10.3389/fneur.2019.00198.
53. Inglese M, Makani S, Johnson G, Cohen BA, Silver JA, Gonen O, et al. Diffuse axonal injury in mild traumatic brain injury: a diffusion tensor imaging study. J Neurosurg. 2005;103(2):298–303. https://doi.org/10.3171/jns.2005.103.2.0298.
54. Meythaler JM, Peduzzi JD, Eleftheriou E, Novack TA. Current concepts: diffuse axonal injury-associated traumatic brain injury. Arch Phys Med Rehabil. 2001;82(10):1461–71. https://doi.org/10.1053/apmr.2001.25137.
55. Mesfin FB, Gupta N, Hays Shapshak A, Taylor RS. Diffuse Axonal Injury (DAI). Treasure Island (FL): StatPearls; 2020.
56. Alexander AL, Lee JE, Lazar M, Field AS. Diffusion tensor imaging of the brain. Neurotherapeutics. 2007;4(3):316–29. https://doi.org/10.1016/j.nurt.2007.05.011.
57. Alves GS, O'Dwyer L, Jurcoane A, Oertel-Knochel V, Knochel C, Prvulovic D, et al. Different patterns of white matter degeneration using multiple diffusion indices and volumetric data in mild cognitive impairment and Alzheimer patients. PLoS One. 2012;7(12):e52859. https://doi.org/10.1371/journal.pone.0052859.
58. Amlien IK, Fjell AM. Diffusion tensor imaging of white matter degeneration in Alzheimer's disease and mild cognitive impairment. Neuroscience. 2014;276:206–15. https://doi.org/10.1016/j.neuroscience.2014.02.017.
59. Chua TC, Wen W, Slavin MJ, Sachdev PS. Diffusion tensor imaging in mild cognitive impairment and Alzheimer's disease: a review. Curr Opin Neurol. 2008;21(1):83–92. https://doi.org/10.1097/WCO.0b013e3282f4594b.
60. Kim YJ, Kwon HK, Lee JM, Kim YJ, Kim HJ, Jung NY, et al. White matter microstructural changes in pure Alzheimer's disease and subcortical vascular dementia. Eur J Neurol. 2015;22(4):709–16. https://doi.org/10.1111/ene.12645.
61. Lee SH, Coutu JP, Wilkens P, Yendiki A, Rosas HD, Salat DH, et al. Tract-based analysis of white matter

degeneration in Alzheimer's disease. Neuroscience. 2015;301:79–89. https://doi.org/10.1016/j.neuroscience.2015.05.049.
62. Bozzali M, Falini A, Franceschi M, Cercignani M, Zuffi M, Scotti G, et al. White matter damage in Alzheimer's disease assessed in vivo using diffusion tensor magnetic resonance imaging. J Neurol Neurosurg Psychiatry. 2002;72(6):742–6. https://doi.org/10.1136/jnnp.72.6.742.
63. Su E, Bell M. Diffuse Axonal Injury. In: Laskowitz D, Grant G, editors. Translational research in traumatic brain injury. Boca Raton (FL): Frontiers in Neuroscience; 2016.
64. Vik A, Kvistad KA, Skandsen T, Ingebrigtsen T. Diffuse axonal injury in traumatic brain injury. Tidsskr Nor Laegeforen. 2006;126(22):2940–4.
65. Parizel PM, Ozsarlak, Van Goethem JW, van den Hauwe L, Dillen C, Verlooy J, et al. Imaging findings in diffuse axonal injury after closed head trauma. Eur Radiol. 1998;8(6):960–5. https://doi.org/10.1007/s003300050496.
66. Arfanakis K, Haughton VM, Carew JD, Rogers BP, Dempsey RJ, Meyerand ME. Diffusion tensor MR imaging in diffuse axonal injury. AJNR Am J Neuroradiol. 2002;23(5):794–802.
67. DeKosky ST, Asken BM. Injury cascades in TBI-related neurodegeneration. Brain Inj. 2017;31(9):1177–82. https://doi.org/10.1080/02699052.2017.1312528.
68. Geng X, Gouttard S, Sharma A, Gu H, Styner M, Lin W, et al. Quantitative tract-based white matter development from birth to age 2 years. Neuroimage. 2012;61(3):542–57. https://doi.org/10.1016/j.neuroimage.2012.03.057.
69. Gilmore JH, Lin W, Corouge I, Vetsa YS, Smith JK, Kang C, et al. Early postnatal development of corpus callosum and corticospinal white matter assessed with quantitative tractography. AJNR Am J Neuroradiol. 2007;28(9):1789–95. https://doi.org/10.3174/ajnr.a0751.
70. Wang S, Ledig C, Hajnal JV, Counsell SJ, Schnabel JA, Deprez M. Quantitative assessment of myelination patterns in preterm neonates using T2-weighted MRI. Sci Rep. 2019;9(1):12938. https://doi.org/10.1038/s41598-019-49350-3.
71. Lye TC, Shores EA. Traumatic brain injury as a risk factor for Alzheimer's disease: a review. Neuropsychol Rev. 2000;10(2):115–29. https://doi.org/10.1023/a:1009068804787.
72. Van Den Heuvel C, Thornton E, Vink R. Traumatic brain injury and Alzheimer's disease: a review. Prog Brain Res. 2007;161:303–16. https://doi.org/10.1016/S0079-6123(06)61021-2.
73. Azouvi P, Arnould A, Dromer E, Vallat-Azouvi C. Neuropsychology of traumatic brain injury: an expert overview. Rev Neurol (Paris). 2017;173(7-8):461–72. https://doi.org/10.1016/j.neurol.2017.07.006.
74. Wang B, Liu W, Prastawa M, Irimia A, Vespa PM, van Horn JD, et al. 4d active cut: an interactive tool for pathological anatomy modeling. Proc IEEE Int Symp Biomed Imaging. 2014;2014:529–32. https://doi.org/10.1109/ISBI.2014.6867925.
75. Rutgers DR, Toulgoat F, Cazejust J, Fillard P, Lasjaunias P, Ducreux D. White matter abnormalities in mild traumatic brain injury: a diffusion tensor imaging study. AJNR Am J Neuroradiol. 2008;29(3):514–9. https://doi.org/10.3174/ajnr.A0856.
76. Lepage C, de Pierrefeu A, Koerte IK, Coleman MJ, Pasternak O, Grant G, et al. White matter abnormalities in mild traumatic brain injury with and without post-traumatic stress disorder: a subject-specific diffusion tensor imaging study. Brain Imaging Behav. 2018;12(3):870–81. https://doi.org/10.1007/s11682-017-9744-5.
77. Parente DB, Gasparetto EL, da Cruz LC, Jr., Domingues RC, Baptista AC, Carvalho AC et al. Potential role of diffusion tensor MRI in the differential diagnosis of mild cognitive impairment and Alzheimer's disease. AJR Am J Roentgenol. 2008;190(5):1369–74. https://doi.org/10.2214/AJR.07.2617.
78. Naggara O, Oppenheim C, Rieu D, Raoux N, Rodrigo S, Dalla Barba G, et al. Diffusion tensor imaging in early Alzheimer's disease. Psychiatry Res. 2006;146(3):243–9. https://doi.org/10.1016/j.pscychresns.2006.01.005.
79. Hinkebein JH, Martin TA, Callahan CD, Johnstone B. Traumatic brain injury and Alzheimer's: deficit profile similarities and the impact of normal ageing. Brain Inj. 2003;17(12):1035–42. https://doi.org/10.1080/0269905031000110490.
80. Dall'Acqua P, Johannes S, Mica L, Simmen HP, Glaab R, Fandino J, et al. Functional and structural network recovery after mild traumatic brain injury: a 1-year longitudinal study. Front Hum Neurosci. 2017;11:280. https://doi.org/10.3389/fnhum.2017.00280.
81. Perry RJ, Hodges JR. Attention and executive deficits in Alzheimer's disease. A critical review. Brain. 1999;122(Pt 3):383–404. https://doi.org/10.1093/brain/122.3.383.
82. McDonald BC, Saykin AJ, McAllister TW. Functional MRI of mild traumatic brain injury (mTBI): progress and perspectives from the first decade of studies. Brain Imaging Behav. 2012;6(2):193–207. https://doi.org/10.1007/s11682-012-9173-4.
83. Cazalis F, Babikian T, Giza C, Copeland S, Hovda D, Asarnow RF. Pivotal role of anterior cingulate cortex in working memory after traumatic brain injury in youth. Front Neurol. 2011;1:158. https://doi.org/10.3389/fneur.2010.00158.
84. Porcelli S, Van Der Wee N, van der Werff S, Aghajani M, Glennon JC, van Heukelum S, et al. Social brain, social dysfunction and social withdrawal. Neurosci Biobehav Rev. 2019;97:10–33. https://doi.org/10.1016/j.neubiorev.2018.09.012.
85. Lalonde G, Bernier A, Beaudoin C, Gravel J, Beauchamp MH. Investigating social functioning after early mild TBI: the quality of parent-child interactions. J Neuropsychol. 2018;12(1):1–22. https://doi.org/10.1111/jnp.12104.
86. Temkin NR, Corrigan JD, Dikmen SS, Machamer J. Social functioning after traumatic brain injury. J Head Trauma Rehabil. 2009;24(6):460–7. https://doi.org/10.1097/HTR.0b013e3181c13413.
87. Gomez-Hernandez R, Max JE, Kosier T, Paradiso S, Robinson RG. Social impairment and depression after traumatic brain injury. Arch Phys Med Rehabil. 1997;78(12):1321–6. https://doi.org/10.1016/s0003-9993(97)90304-x.
88. Bediou B, Ryff I, Mercier B, Milliery M, Henaff MA, D'Amato T, et al. Impaired social cognition in mild Alzheimer disease. J Geriatr Psychiatry Neurol.

2009;22(2):130–40. https://doi.org/10.1177/0891988709332939.
89. Gilmour G, Porcelli S, Bertaina-Anglade V, Arce E, Dukart J, Hayen A, et al. Relating constructs of attention and working memory to social withdrawal in Alzheimer's disease and schizophrenia: issues regarding paradigm selection. Neurosci Biobehav Rev. 2019;97:47–69. https://doi.org/10.1016/j.neubiorev.2018.09.025.
90. Calvillo M, Irimia A. Neuroimaging and psychometric assessment of mild cognitive impairment after traumatic brain injury. Front Psychol. 2020;11:1423. https://doi.org/10.3389/fpsyg.2020.01423.
91. Shaver TK, Ozga JE, Zhu B, Anderson KG, Martens KM, Vonder HC. Long-term deficits in risky decision-making after traumatic brain injury on a rat analog of the Iowa gambling task. Brain Res. 1704;2019:103–13. https://doi.org/10.1016/j.brainres.2018.10.004.
92. Ozga-Hess JE, Whirtley C, O'Hearn C, Pechacek K, Vonder HC. Unilateral parietal brain injury increases risk-taking on a rat gambling task. Exp Neurol. 2020;327:113217. https://doi.org/10.1016/j.expneurol.2020.113217.
93. Cotrena C, Branco LD, Zimmermann N, Cardoso CO, Grassi-Oliveira R, Fonseca RP. Impaired decision-making after traumatic brain injury: the Iowa Gambling Task. Brain Inj. 2014;28(8):1070–5. https://doi.org/10.3109/02699052.2014.896943.
94. Levin HS, Wilde E, Troyanskaya M, Petersen NJ, Scheibel R, Newsome M, et al. Diffusion tensor imaging of mild to moderate blast-related traumatic brain injury and its sequelae. J Neurotrauma. 2010;27(4):683–94. https://doi.org/10.1089/neu.2009.1073.
95. Sinha S, Tiwari SC, Shah S, Singh P, Tripathi SM, Pandey N, et al. Neural bases of impaired decision making process in Alzheimer's disease. Society of Applied Neurosciences 2016; 6 Oct - 9 Oct. Corfu, Greece: Frontiers; 2016.
96. Niogi SN, Mukherjee P, Ghajar J, Johnson C, Kolster RA, Sarkar R, et al. Extent of microstructural white matter injury in postconcussive syndrome correlates with impaired cognitive reaction time: a 3T diffusion tensor imaging study of mild traumatic brain injury. AJNR Am J Neuroradiol. 2008;29(5):967–73. https://doi.org/10.3174/ajnr.A0970.
97. Yin B, Li DD, Huang H, Gu CH, Bai GH, Hu LX, et al. Longitudinal changes in diffusion tensor imaging following mild traumatic brain injury and correlation with outcome. Front Neural Circuits. 2019;13:28. https://doi.org/10.3389/fncir.2019.00028.
98. Alhilali LM, Yaeger K, Collins M, Fakhran S. Detection of central white matter injury underlying vestibulopathy after mild traumatic brain injury. Radiology. 2014;272(1):224–32. https://doi.org/10.1148/radiol.14132670.
99. Duering M, Gesierich B, Seiler S, Pirpamer L, Gonik M, Hofer E, et al. Strategic white matter tracts for processing speed deficits in age-related small vessel disease. Neurology. 2014;82(22):1946–50. https://doi.org/10.1212/WNL.0000000000000475.
100. McInnes K, Friesen CL, MacKenzie DE, Westwood DA, Boe SG. Mild traumatic brain injury (mTBI) and chronic cognitive impairment: a scoping review. PLoS One. 2017;12(4):e0174847. https://doi.org/10.1371/journal.pone.0174847.
101. Konrad C, Geburek AJ, Rist F, Blumenroth H, Fischer B, Husstedt I, et al. Long-term cognitive and emotional consequences of mild traumatic brain injury. Psychol Med. 2011;41(6):1197–211. https://doi.org/10.1017/S0033291710001728.
102. Johansson B, Andrell P, Ronnback L, Mannheimer C. Follow-up after 5.5 years of treatment with methylphenidate for mental fatigue and cognitive function after a mild traumatic brain injury. Brain Inj. 2020;34(2):229–35. https://doi.org/10.1080/02699052.2019.1683898.
103. Mathias JL, Beall JA, Bigler ED. Neuropsychological and information processing deficits following mild traumatic brain injury. J Int Neuropsychol Soc. 2004;10(2):286–97. https://doi.org/10.1017/S1355617704102117.
104. Jonasson A, Levin C, Renfors M, Strandberg S, Johansson B. Mental fatigue and impaired cognitive function after an acquired brain injury. Brain Behav. 2018;8(8):e01056. https://doi.org/10.1002/brb3.1056.
105. Belmont A, Agar N, Azouvi P. Subjective fatigue, mental effort, and attention deficits after severe traumatic brain injury. Neurorehabil Neural Repair. 2009;23(9):939–44. https://doi.org/10.1177/1545968309340327.
106. Ziino C, Ponsford J. Selective attention deficits and subjective fatigue following traumatic brain injury. Neuropsychology. 2006;20(3):383–90. https://doi.org/10.1037/0894-4105.20.3.383.
107. Hillary FG, Genova HM, Medaglia JD, Fitzpatrick NM, Chiou KS, Wardecker BM, et al. The nature of processing speed deficits in traumatic brain injury: is less brain more? Brain Imaging Behav. 2010;4(2):141–54. https://doi.org/10.1007/s11682-010-9094-z.
108. Nestor PG, Parasuraman R, Haxby JV. Speed of information processing and attention in early Alzheimer's dementia. Dev Neuropsychol. 2009;7(2):243–56. https://doi.org/10.1080/87565649109540491.
109. Warkentin S, Erikson C, Janciauskiene S. rCBF pathology in Alzheimer's disease is associated with slow processing speed. Neuropsychologia. 2008;46(5):1193–200. https://doi.org/10.1016/j.neuropsychologia.2007.08.029.
110. Croall ID, Cowie CJ, He J, Peel A, Wood J, Aribisala BS, et al. White matter correlates of cognitive dysfunction after mild traumatic brain injury. Neurology. 2014;83(6):494–501. https://doi.org/10.1212/WNL.0000000000000666.
111. Kircher T, Nagels A, Kirner-Veselinovic A, Krach S. Neural correlates of rhyming vs. lexical and semantic fluency. Brain Res. 2011;1391:71–80. https://doi.org/10.1016/j.brainres.2011.03.054.
112. Paek EJ, Murray LL, Newman SD. Neural correlates of verb fluency performance in cognitively healthy older adults and individuals with dementia: a pilot fMRI study. Front Aging Neurosci. 2020;12:73. https://doi.org/10.3389/fnagi.2020.00073.
113. Kave G, Heled E, Vakil E, Agranov E. Which verbal fluency measure is most useful in demonstrating executive deficits after traumatic brain injury? J Clin Exp Neuropsychol. 2011;33(3):358–65. https://doi.org/10.1080/13803395.2010.518703.
114. Henry JD, Crawford JR. A meta-analytic review of verbal fluency performance in patients with traumatic brain injury. Neuropsychology. 2004;18(4):621–8. https://doi.org/10.1037/0894-4105.18.4.621.

115. Mathias JL, Coats JL. Emotional and cognitive sequelae to mild traumatic brain injury. J Clin Exp Neuropsychol. 1999;21(2):200–15. https://doi.org/10.1076/jcen.21.2.200.930.
116. Voller B, Benke T, Benedetto K, Schnider P, Auff E, Aichner F. Neuropsychological, MRI and EEG findings after very mild traumatic brain injury. Brain Inj. 1999;13(10):821–7. https://doi.org/10.1080/026990599121214.
117. Henry JD, Crawford JR, Phillips LH. Verbal fluency performance in dementia of the Alzheimer's type: a meta-analysis. Neuropsychologia. 2004;42(9):1212–22. https://doi.org/10.1016/j.neuropsychologia.2004.02.001.
118. Kljajevic V. Verbal fluency and intrinsic brain activity in Alzheimer's disease. Croat Med J. 2015;56(6):573–7. https://doi.org/10.3325/cmj.2015.56.573.
119. Melrose RJ, Campa OM, Harwood DG, Osato S, Mandelkern MA, Sultzer DL. The neural correlates of naming and fluency deficits in Alzheimer's disease: an FDG-PET study. Int J Geriatr Psychiatry. 2009;24(8):885–93. https://doi.org/10.1002/gps.2229.
120. Brun A, Englund E. Regional pattern of degeneration in Alzheimer's disease: neuronal loss and histopathological grading. Histopathology. 1981;5(5):549–64. https://doi.org/10.1111/j.1365-2559.1981.tb01818.x.
121. Collette F, Van der Linden M, Salmon E. Executive dysfunction in Alzheimer's disease. Cortex. 1999;35(1):57–72. https://doi.org/10.1016/s0010-9452(08)70785-8.
122. Guarino A, Favieri F, Boncompagni I, Agostini F, Cantone M, Casagrande M. Executive functions in Alzheimer Disease: a systematic review. Front Aging Neurosci. 2018;10:437. https://doi.org/10.3389/fnagi.2018.00437.
123. Ozga JE, Povroznik JM, Engler-Chiurazzi EB, Vonder HC. Executive (dys)function after traumatic brain injury: special considerations for behavioral pharmacology. Behav Pharmacol. 2018;29(7):617–37. https://doi.org/10.1097/FBP.0000000000000430.
124. Cossette I, Gagne ME, Ouellet MC, Fait P, Gagnon I, Sirois K, et al. Executive dysfunction following a mild traumatic brain injury revealed in early adolescence with locomotor-cognitive dual-tasks. Brain Inj. 2016;30(13-14):1648–55. https://doi.org/10.1080/02699052.2016.1200143.
125. Miles L, Grossman RI, Johnson G, Babb JS, Diller L, Inglese M. Short-term DTI predictors of cognitive dysfunction in mild traumatic brain injury. Brain Inj. 2008;22(2):115–22. https://doi.org/10.1080/02699050801888816.
126. Shum D, Gill H, Banks M, Maujean A, Griffin J, Ward H. Planning ability following moderate to severe traumatic brain injury: performance on a 4-disk version of the Tower of London. Brain Impairment. 2009;10(3):320–4. https://doi.org/10.1375/brim.10.3.320.
127. Brooks J, Fos LA, Greve KW, Hammond JS. Assessment of executive function in patients with mild traumatic brain injury. J Trauma. 1999;46(1):159–63. https://doi.org/10.1097/00005373-199901000-00027.
128. Lange KW, Sahakian BJ, Quinn NP, Marsden CD, Robbins TW. Comparison of executive and visuospatial memory function in Huntington's disease and dementia of Alzheimer type matched for degree of dementia. J Neurol Neurosurg Psychiatry. 1995;58(5):598–606. https://doi.org/10.1136/jnnp.58.5.598.
129. Satler C, Guimaraes L, Tomaz C. Planning ability impairments in probable Alzheimer's disease patients: evidence from the Tower of London test. Dement Neuropsychol. 2017;11(2):137–44. https://doi.org/10.1590/1980-57642016dn11-020006.
130. Mack JL, Patterson MB. Executive dysfunction and Alzheimer's disease: performance on a test of planning ability, the Porteus Maze Test. Neuropsychology. 1995;9(4):556–64. https://doi.org/10.1037/0894-4105.9.4.556.
131. Marco EJ, Harrell KM, Brown WS, Hill SS, Jeremy RJ, Kramer JH, et al. Processing speed delays contribute to executive function deficits in individuals with agenesis of the corpus callosum. J Int Neuropsychol Soc. 2012;18(3):521–9. https://doi.org/10.1017/S1355617712000045.
132. Hinkley LB, Marco EJ, Findlay AM, Honma S, Jeremy RJ, Strominger Z, et al. The role of corpus callosum development in functional connectivity and cognitive processing. PLoS One. 2012;7(8):e39804. https://doi.org/10.1371/journal.pone.0039804.
133. Shin G, Kim C. Neural correlates of cognitive style and flexible cognitive control. Neuroimage. 2015;113:78–85. https://doi.org/10.1016/j.neuroimage.2015.03.046.
134. Leunissen I, Coxon JP, Caeyenberghs K, Michiels K, Sunaert S, Swinnen SP. Subcortical volume analysis in traumatic brain injury: the importance of the fronto-striato-thalamic circuit in task switching. Cortex. 2014;51:67–81. https://doi.org/10.1016/j.cortex.2013.10.009.
135. Hawley C, Sakr M, Scapinello S, Salvo J, Wrenn P. Traumatic brain injuries in older adults-6 years of data for one UK trauma centre: retrospective analysis of prospectively collected data. Emerg Med J. 2017;34(8):509–16. https://doi.org/10.1136/emermed-2016-206506.
136. Mosenthal AC, Livingston DH, Lavery RF, Knudson MM, Lee S, Morabito D, et al. The effect of age on functional outcome in mild traumatic brain injury: 6-month report of a prospective multicenter trial. J Trauma. 2004;56(5):1042–8. https://doi.org/10.1097/01.ta.0000127767.83267.33.
137. Centers for Disease Control and Prevention. Trends in aging–United States and worldwide. MMWR Morb Mortal Wkly Rep. 2003;52(6):101–4, 6.
138. Thompson HJ, Dikmen S, Temkin N. Prevalence of comorbidity and its association with traumatic brain injury and outcomes in older adults. Res Gerontol Nurs. 2012;5(1):17–24. https://doi.org/10.3928/19404921-20111206-02.
139. Burgmans S, van Boxtel MP, Gronenschild EH, Vuurman EF, Hofman P, Uylings HB, et al. Multiple indicators of age-related differences in cerebral white matter and the modifying effects of hypertension. Neuroimage. 2010;49(3):2083–93. https://doi.org/10.1016/j.neuroimage.2009.10.035.
140. Liu JY, Zhou YJ, Zhai FF, Han F, Zhou LX, Ni J, et al. Cerebral microbleeds are associated with loss of white matter integrity. AJNR Am J Neuroradiol. 2020;41(8):1397–404. https://doi.org/10.3174/ajnr.A6622.
141. Iscan Z, Jin TB, Kendrick A, Szeglin B, Lu H, Trivedi M, et al. Test-retest reliability of freesurfer measurements within and between sites: effects of visual approval process.

Human Brain Mapping. 2015;36(9):3472–85. https://doi.org/10.1002/hbm.22856.

142. Irimia A, Van Horn JD, Vespa PM. Cerebral microhemorrhages due to traumatic brain injury and their effects on the aging human brain. Neurobiology of Aging. 2018;66:158–64.
143. Oishi K, Zilles K, Amunts K, Faria A, Jiang H, Li X, et al. Human brain white matter atlas: identification and assignment of common anatomical structures in superficial white matter. Neuroimage. 2008;43(3):447–57. https://doi.org/10.1016/j.neuroimage.2008.07.009.
144. Fortin JP, Cullen N, Sheline YI, Taylor WD, Aselcioglu I, Cook PA, et al. Harmonization of cortical thickness measurements across scanners and sites. Neuroimage. 2018;167:104–20. https://doi.org/10.1016/j.neuroimage.2017.11.024.
145. Fortin JP, Parker D, Tunc B, Watanabe T, Elliott MA, Ruparel K, et al. Harmonization of multi-site diffusion tensor imaging data. Neuroimage. 2017;161:149–70. https://doi.org/10.1016/j.neuroimage.2017.08.047.
146. Johnson WE, Li C, Rabinovic A. Adjusting batch effects in microarray expression data using empirical Bayes methods. Biostatistics. 2007;8(1):118–27. https://doi.org/10.1093/biostatistics/kxj037.